JGR Oceans

RESEARCH ARTICLE
10.1029/2023JC020583

Arctic Freshwater Sources and Ocean Mixing Relationships Revealed With Seawater Isotopic Tracing

Ben G. Kopec[1], Eric S. Klein[2], Gene C. Feldman[3], Shawn A. Pedron[4], Hannah Bailey[5], Douglas Causey[6,7], Alun Hubbard[8,9], Hannu Marttila[5], and Jeffrey M. Welker[6,10,11]

[1]Great Lakes Research Center, Michigan Technological University, Houghton, MI, USA, [2]Geological Sciences, University of Alaska Anchorage, Anchorage, AK, USA, [3]NASA Goddard Space Flight Center, Greenbelt, MD, USA, [4]Earth System Science, University of California Irvine, Irvine, CA, USA, [5]Water, Energy and Environmental Engineering, University of Oulu, Oulu, Finland, [6]Biological Sciences, University of Alaska Anchorage, Anchorage, AK, USA, [7]Harvard Kennedy School, Belfer Center Arctic Initiative, Harvard University, Cambridge, MA, USA, [8]Centre for Ice, Cryosphere, Carbon and Climate, Institute for Geosciences, UiT—The Arctic University of Norway, Tromsø, Norway, [9]Geography Research Unit, University of Oulu, Oulu, Finland, [10]Ecology and Genetics Research Unit, University of Oulu, Oulu, Finland, [11]The University of the Arctic (UArctic), Rovaniemi, Finland

Abstract The Arctic Ocean and adjacent seas are undergoing increased freshwater influx due to enhanced glacial and sea ice melt, precipitation, and runoff. Accurate delineation of these freshwater sources is vital as they critically modulate ocean composition and circulation with widespread and varied impacts. Despite this, the delineation of freshwater sources using physical oceanographic measurements (e.g., temperature, salinity) alone is challenging and there is a requirement to improve the partitioning of ocean water masses and their mixing relationships. Here, we complement traditional oceanographic measurements with continuous surface seawater isotopic analysis ($\delta^{18}O$ and deuterium excess) across a transect extending from coastal Alaska to Baffin Bay and the Labrador Sea conducted from the US Coast Guard Cutter Healy in Autumn 2021. We find that the diverse isotopic signatures of Arctic freshwater sources, coupled with the high freshwater proportion in these marine systems, facilitates detailed fingerprinting and partitioning. We observe the highest freshwater composition in the Beaufort Sea and Amundsen Gulf regions, with heightened freshwater content in eastern Baffin Bay adjacent to West Greenland. We apply isotopic analysis to delineate freshwater sources, revealing that in the Western Arctic freshwater inputs are dominated by meteoric water inputs—specifically the Mackenzie River—with a smaller sea ice meltwater component and in Baffin Bay the primary sources are local precipitation and glacial meltwater discharge. We demonstrate that such freshwater partitioning cannot be achieved using temperature-salinity relationships alone, and highlight the potential of seawater isotopic tracers to assess the roles and importance of these evolving freshwater sources.

Plain Language Summary Freshwater inputs to the Arctic seas, including glacial and sea ice meltwater, precipitation, and river runoff, are increasing as the Arctic warms. The impacts of these changing freshwater influxes are varied depending on the type of freshwater source, and thus it is important to delineate and trace these different freshwater sources, which represents a significant challenge using only traditional physical oceanographic measurements (e.g., temperature, salinity). In this study, we utilize a new approach to identify and trace freshwater sources using continuous seawater isotopic measurements during a cruise extending from coastal Alaska, through the Canadian Archipelago, and across Baffin Bay and the Labrador Sea. We show that these isotopic measurements, which have been commonly used in other media (e.g., precipitation, water vapor, ice cores), hold important and distinct information about the source and mixing of different freshwater sources. We use these measurements to identify the freshwater sources (e.g., Mackenzie vs. Yukon River) contributing to ocean surface waters across the Arctic region.

Key Points:

- Seawater isotopic measurements ($\delta^{18}O$, $\delta^{2}H$, deuterium excess) show heightened freshwater content in the Beaufort Sea and Baffin Bay
- Isotopic observations enable freshwater source delineation not feasible from traditional physical oceanographic methods
- Freshwater source delineation includes the Mackenzie and Yukon Rivers around coastal Alaska and glacial meltwater in Baffin Bay

Supporting Information:

Supporting Information may be found in the online version of this article.

Correspondence to:

B. G. Kopec,
bkopec@mtu.edu

Citation:

Kopec, B. G., Klein, E. S., Feldman, G. C., Pedron, S. A., Bailey, H., Causey, D., et al. (2024). Arctic freshwater sources and ocean mixing relationships revealed with seawater isotopic tracing. *Journal of Geophysical Research: Oceans*, *129*, e2023JC020583. https://doi.org/10.1029/2023JC020583

Received 10 OCT 2023
Accepted 13 JUN 2024

Author Contributions:

Conceptualization: Ben G. Kopec, Eric S. Klein, Jeffrey M. Welker
Data curation: Ben G. Kopec, Eric S. Klein, Gene C. Feldman, Jeffrey M. Welker
Formal analysis: Ben G. Kopec, Eric S. Klein, Gene C. Feldman, Shawn A. Pedron, Hannah Bailey, Douglas Causey, Alun Hubbard, Hannu Marttila, Jeffrey M. Welker
Funding acquisition: Ben G. Kopec, Eric S. Klein, Hannah Bailey, Douglas Causey, Alun Hubbard, Hannu Marttila, Jeffrey M. Welker
Investigation: Ben G. Kopec, Eric S. Klein, Gene C. Feldman, Shawn A. Pedron, Hannah Bailey, Douglas Causey, Alun Hubbard, Hannu Marttila, Jeffrey M. Welker
Methodology: Ben G. Kopec, Eric S. Klein, Gene C. Feldman, Shawn

1. Introduction

Arctic seas are fundamentally changing, including variations in the physical and chemical composition of seawater (Polyakov et al., 2018), shifts in circulation at all depths (Morison et al., 2021; Timmermans & Marshall, 2020; Woodgate, 2018), new ocean-atmosphere interactions due to the loss of sea ice (Bailey et al., 2021; Meneghello et al., 2018; Polyakov et al., 2017), new sources and redistribution of nutrients and organic matter (Codispoti et al., 2013; Strauss et al., 2022; Terhaar et al., 2021), and altered biological productivity (Arrigo and van Dijken, 2015; Farmer et al., 2021; Holding et al., 2015; Lewis et al., 2020), driven in

A. Pedron, Hannah Bailey, Douglas Causey, Alun Hubbard, Hannu Marttila, Jeffrey M. Welker
Project administration: Eric S. Klein, Jeffrey M. Welker
Resources: Ben G. Kopec, Eric S. Klein, Gene C. Feldman, Shawn A. Pedron, Hannah Bailey, Douglas Causey, Alun Hubbard, Hannu Marttila, Jeffrey M. Welker
Supervision: Eric S. Klein, Shawn A. Pedron, Jeffrey M. Welker
Validation: Ben G. Kopec, Eric S. Klein, Gene C. Feldman, Shawn A. Pedron, Hannah Bailey, Douglas Causey, Alun Hubbard, Hannu Marttila, Jeffrey M. Welker
Visualization: Ben G. Kopec, Eric S. Klein, Gene C. Feldman, Shawn A. Pedron, Hannah Bailey, Douglas Causey, Alun Hubbard, Hannu Marttila, Jeffrey M. Welker
Writing – original draft: Ben G. Kopec
Writing – review & editing: Ben G. Kopec, Eric S. Klein, Gene C. Feldman, Shawn A. Pedron, Hannah Bailey, Douglas Causey, Alun Hubbard, Hannu Marttila, Jeffrey M. Welker

large part by enhanced Arctic warming of almost four times the global mean (Rantanen et al., 2022). These shifts are influenced by a changing Arctic water cycle that is leading to greater freshwater influxes to Arctic seas, including by terrestrial surface (e.g., river) runoff (Feng et al., 2021) and by glacially-derived meltwater (Bamber et al., 2012; Box et al., 2022; Karlsson et al., 2021), which is increasing and shifting the distribution of freshwater content of these waters (Carmack et al., 2016; Zhang et al., 2021). Because of these shifts, it is critical to delineate these water masses and identify their mixing relationships to improve understanding of the varied impacts of freshwater both now and in the future. Despite this, partitioning of different freshwater sources can be challenging using salinity and temperature measurements alone (e.g., Huhn et al., 2021), and in this study, we apply novel stable water isotope analysis to facilitate the task. Additionally, rarely are these freshwater sources and processes collectively documented in situ during defined time periods across large swaths of the Arctic seas, limiting our understanding of their impact on changes in water masses and their spatial variations across the Arctic.

Tracing freshwater influxes and their spatial impacts is possible through the measurement of stable water isotope ratios of oxygen ($\delta^{18}O$) and hydrogen ($\delta^{2}H$) in seawater, where the focus is predominately on the $\delta^{18}O$ values as a measure of freshwater composition (e.g., Bauch et al., 1995). Global surface seawater averages vary between −1 and 1‰ for $\delta^{18}O$ (e.g., LeGrande & Schmidt, 2006; Schmidt et al., 2007). However, observations of Arctic seawater have shown excursions to more negative $\delta^{18}O$ values due to high influxes of freshwater runoff and glacial melt with very low $\delta^{18}O$ values (e.g., Bauch et al., 2005; Bonne et al., 2019; Charette et al., 2020; Cooper et al., 2022; Henson et al., 2023; Klein et al., 2024; Macdonald et al., 1995). These seawater $\delta^{18}O$ values are typically strongly positively correlated with salinity (e.g., Bauch et al., 2005; MacLachlan et al., 2007), and thus these corresponding low salinities and negative $\delta^{18}O$ values represent higher freshwater content.

Rarely used in Arctic seawater isotope geochemistry studies is an additional identifier of freshwater—deuterium excess (*d-excess* or *d*; $d = \delta^{2}H - 8 \cdot \delta^{18}O$; Dansgaard, 1964). This second-order isotope parameter provides an additional means by which to identify and partition different water masses and freshwater sources. The key focus in this study is to use *d-excess* measurements together with $\delta^{18}O$ observations to separate distinct freshwater sources from one another. To effectively delineate these freshwater sources: (a) the freshwater content needs to be sufficiently high in total proportion of the measured seawater, and (b) the isotopic composition of the different freshwater sources is unique from one another. Fortunately, in the Arctic, this is the case for many of these sources, where numerous waters have been previously measured, including precipitation (e.g., Kopec et al., 2016; Mellat et al., 2021; Putman et al., 2017), river runoff (e.g., Gibson et al., 2020; The Arctic Great Rivers Observatory, 2024; Yi et al., 2010), and glacial meltwater (e.g., Csank et al., 2019; Kopec et al., 2018). Very few oceanographic studies have utilized seawater *d-excess* observations, but in one example that does, Dubinina et al. (2019) use *d-excess* measurements to delineate glacial meltwater from river water in the water column in two bays of the Novaya Zemlya Archipelago.

Moreover, new technological advancements allow continuous collection and analysis of seawater isotopes (Klein et al., 2024), providing high temporal resolution that yields new insights not apparent from discrete sampling methods. While the Dubinina et al. (2019) study is possible with relatively small discrete sample size ($n = 19$ for their *d-excess* observations) given the constrained physical systems being investigated, discrete sampling inherently limits the spatial and temporal scope of work. Continuous measurements can significantly enhance the spatial scope and resolution of understanding (Klein et al., 2024), such as identifying which freshwater source dominates a given ocean water mass and allow for the tracing of surface circulation around a given region.

Here, we examine continuous seawater isotope ($\delta^{18}O$, $\delta^{2}H$, and *d-excess* values) measurements undertaken during an Arctic icebreaker cruise to explore changing freshwater influxes and content. From late August through early October 2021 (Figure 1), we conducted measurements aboard the United States Coast Guard Cutter (USCGC) Healy that transited the Chukchi and Beaufort Seas, the Northwest Passage through the Canadian Archipelago, and performed numerous transects across Baffin Bay and the Labrador Sea, including detailed examinations of several fjords and coastal regions of West Greenland. This cruise track—covering 30° of latitude and 115° of longitude—allowed us to continuously measure the spatial variations and impacts of freshwater inputs at an unprecedented resolution and within a short time-window (40 days), thereby facilitating a like-by-like, meaningful inter-comparison between regions; an approach that minimizes confounding effects of samples collected in different years (e.g., LeGrande & Schmidt, 2006). We use this new seawater isotopic data set to explore $\delta^{18}O$-*d-excess* relationships across the Arctic in the context of other traditional physical oceanographic observations (e.g.,

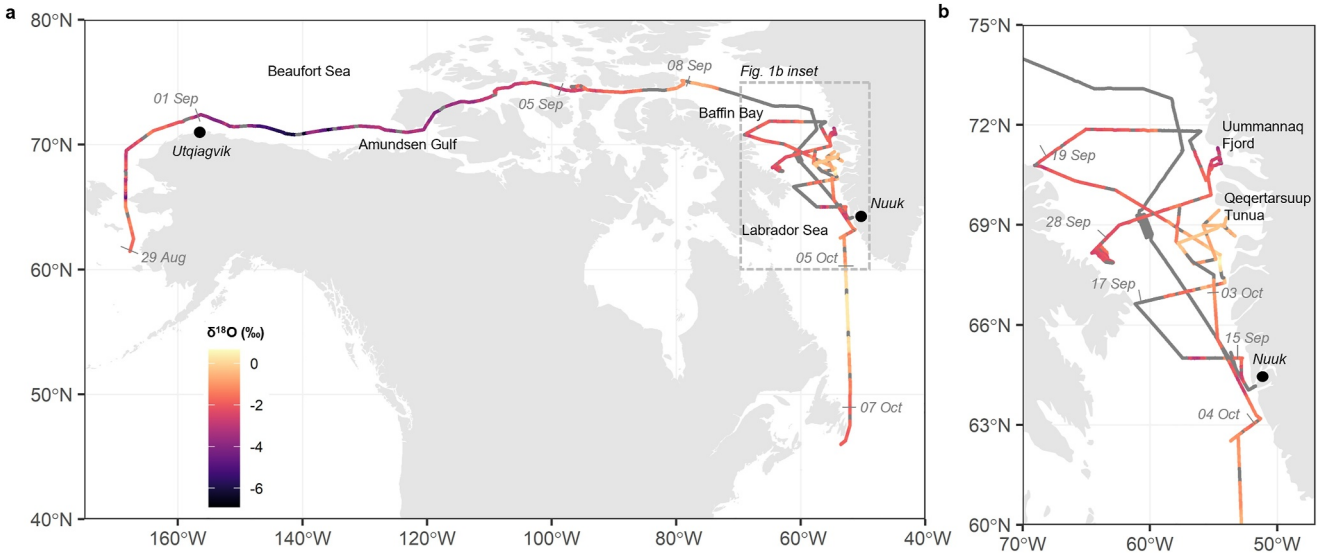

Figure 1. (a) Map of entire United States Coast Guard Cutter Healy autumn 2021 (29 August to 7 October) cruise track and (b) detail of transects in Baffin Bay and Labrador Sea colored by 5-min average $\delta^{18}O$ values; locations with no $\delta^{18}O$ values displayed in gray. Dates labeled along transect are cruise location at 0000 UTC of that day. Timing of other notable locations include Nuuk, Greenland on 13 September, and the inner most transects of Uummannaq Fjord on 24 and 25 September and Qeqertarsuup Tunua (Disko Bugt) on 1 and 2 October.

temperature, salinity), where we: (a) delineate key ocean water masses and (b) partition distinct freshwater inputs and their mixing relationships.

2. Materials and Methods

2.1. Seawater Isotopic Observations and Calibration

Isotopic measurements were carried out aboard the USCGC Healy from 29 August 2021 20:05 UTC to 7 October 2021 10:20 UTC. Using the sample sampling arrangement as Klein et al. (2024), near-surface seawater was continuously sampled through the seawater underway system that draws in water from ~8 m below the surface. Seawater from this continuous flow was subsampled by a Picarro Continuous Water Sampler (CWS). The CWS converts the liquid seawater to water vapor through a diffusive membrane cartridge. Over time, salt accumulates on the CWS membrane cartridge, which required frequent (~weekly) cleaning with deionized water to remove salt build up to ensure high flow rates of water through the CWS (we define the water vapor concentration lower limit to be 9,000 ppmv; measurements below this concentration were excluded from this analysis). The resulting water vapor from the CWS flows through a Picarro L2140-i analyzer to continuously measure the oxygen ($\delta^{18}O$) and hydrogen ($\delta^{2}H$) isotopic composition at 1 Hz resolution (>2,000,000 individual measurements). Isotopic ratios were then calibrated to correct the offset between measured and actual values produced by the CWS method. Deuterium excess (*d-excess*, *d*) was computed from these two calibrated isotopic ratios in the form of $d = \delta^{2}H - 8 \cdot \delta^{18}O$.

Calibrations of the isotopic data are conducted in two primary steps: (a) correction by known standard waters, and (b) correction by discrete samples, including an H_2O concentration correction. This isotopic data is first calibrated using two known standard waters that are run sequentially for 20 min each through the CWS every 12 hr, where the final 5-min window when isotopic measurements have stabilized are used for calibration computations. These standards included Fiji water ($\delta^{18}O = -6.6‰$, $\delta^{2}H = -42.2‰$) and Anchorage Tap Water ($\delta^{18}O = -19.2‰$, $\delta^{2}H = -146.6‰$), and were used to correct any offset between the measured and actual values. A spline fit ($\lambda = 0.001$) of the two standard waters was determined over the length of the cruise and used to calculate the offset between the raw measurement and the actual value. These computed offsets were then applied to the raw seawater measurements to calibrate the data. We refer to the data after this step as "standard-calibrated" data. Because of the nature of the CWS, large differences occurred between the raw measurements and these corrected values, and this difference varied substantially throughout the cruise, so it was critical to perform frequent calibration runs with these standard waters. All isotopic values presented here are computed on the Vienna Standard Mean Ocean

Water-Standard Light Antarctic Precipitation (VSMOW-SLAP) scale. The 30 min after standard runs were excluded due to lasting effects of the low isotopic values of the standard waters.

While these standard waters have relatively low $\delta^{18}O$ and $\delta^{2}H$ values compared to the majority of seawater measured in this study, a large volume of standard water was required to cover the duration of the cruise (>10 L of each) and thus it was not feasible to repeatedly run expensive commercially-available standards (e.g., USGS or IAEA standards) in these quantities. The two standard waters used in this study could be compiled in large quantities at low cost and standardized with repeated testing before and after the cruise. For future experiments, we are assessing more effective ways to run standard waters and gather bulk waters to standardize for this type of analysis. This method clearly results in added uncertainty in the isotopic values, including some unknown uncertainty beyond the standard runs, but we are confident in the analyses presented given the range of natural variability we are examining and further calibration with the discrete sampling protocol described below.

The second calibration step compared discrete seawater samples with the standard-calibrated continuous data to identify additional offsets, finding that the concentration of water vapor reaching the analyzer is a critical factor for this data set. Occasional discrete samples ($n = 65$) were also collected from the underway system throughout the cruise to be analyzed independently of continuous samples. Grab samples were collected in 40 mL High Density Polyethylene (HDPE) bottles and refrigerated until the end of the cruise, when they were shipped to the University of Oulu and analyzed for their isotopic ratios ($\delta^{18}O$ and $\delta^{2}H$) by a Picarro L2140-i. The reference waters used in this analysis included USGS45 ($\delta^{18}O = -2.238‰$, $\delta^{2}H = -10.3‰$) and USGS46 ($\delta^{18}O = -29.80‰$, $\delta^{2}H = -235.8‰$): a range higher than the bulk standard waters used with the CWS (although still not to the full observed seawater range). The analytical uncertainty (1σ) is 0.1‰ for $\delta^{18}O$, 0.5‰ for $\delta^{2}H$, and 0.9‰ for *d-excess*. These discrete samples were compared with the continuous samples shown in Figure S1 in Supporting Information S1, and show a water concentration effect in the continuous measurements that alters the isotopic composition (similar to what is experienced in relatively dry water vapor isotopic measurements—e.g., Steen-Larsen et al., 2013), likely caused by variations in flow through the membrane as salt builds up on the membrane surface. We applied a water vapor concentration correction (Kopec et al., 2022) based on this difference to all continuous samples shown in this study (see Supporting Information S1). Developing a correction based on concentration is important because it is a systematic and predictable effect that we are removing from the data set, as opposed to simply fitting the curve to any given point based solely on the discrete samples. In correcting the seawater measurements based on this concentration effect, we observe significant improvement in achieving a 1:1 relationship between the discrete and continuous measurements. It is also important to note that there is no clear divergence at higher $\delta^{18}O$ or $\delta^{2}H$ values as we get further removed from the standard waters range. This adds confidence in using this seawater isotopic data at higher values without concern of there being major non-linear errors introduced once outside of the standard range. It would be unlikely for a major systematic instrumental shift to occur that affects the $\delta^{18}O$ values within 2‰ (or $\delta^{2}H$ values within 10‰) of the USGS 45 water used in the discrete analysis. Across a range of studies using these techniques, broadly linear relationships between raw isotopic measurements compared to a fully calibrated instrument have been shown repeatedly for the isotopic range in this study, especially when measuring isotopic ratios at the high water vapor concentration levels produced by the CWS and measured in this study (Casado et al., 2016; Steen-Larsen et al., 2013).

Given typical Picarro L2140-i instrument analytical error for both the continuous and discrete samples and error introduced by this discrete-continuous comparison and correction (see Supporting Information S1), we estimate approximate uncertainty (1σ) values to be <0.3‰ for $\delta^{18}O$, <0.9‰ for $\delta^{2}H$, and <2.1‰ for *d-excess*. This uncertainty is largest at higher $\delta^{18}O$ and $\delta^{2}H$ values (when outside standard water range) and at lower water concentration levels.

While there may be more error associated with these continuous observations than the typical discrete samples, particularly for *d-excess*, this error is still smaller than the natural range of variability in the study region and therefore these measurements can be used confidently for certain analyses in this type of marine system. The strong relationship between $\delta^{18}O$ and salinity (Figure 2a) shows that the absolute variations of these continuous $\delta^{18}O$ values can be considered robust for examining freshwater content. Given the greater amount of error in *d-excess* variations compared to the single isotope ratios, relative variations are more robust than absolute ones, but we show that these variations can nevertheless yield insights into composition of surface water masses and mixing relationships. Of particular interest in this study is identifying and partitioning freshwater sources using these seawater observations, which is most reliant on the freshest seawater (lowest $\delta^{18}O$ and $\delta^{2}H$ values) that have the

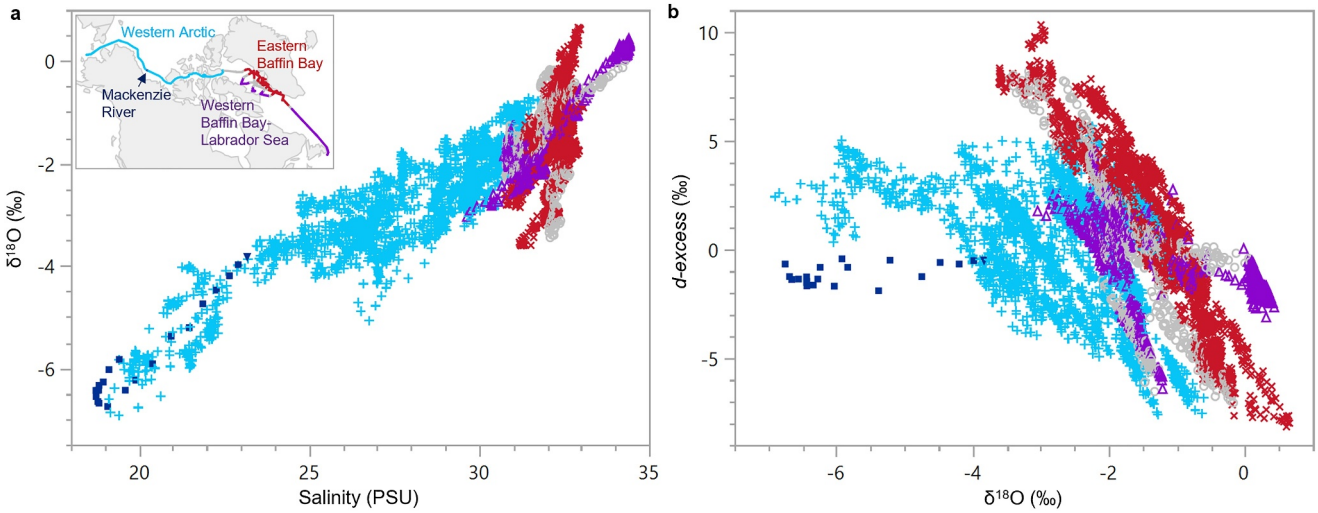

Figure 2. (a) 5-Min average salinity versus $\delta^{18}O$. Data is colored by approximate region as defined in the inset for the following regions: western Arctic (light blue +), Mackenzie River (dark blue ■), western Baffin Bay and Labrador Sea (purple △), Central Baffin Bay (gray), and eastern Baffin Bay (dark red x). (b) 5-Min average $\delta^{18}O$ versus *d-excess*. Data colored as in (a).

lowest uncertainty of the sampled seawaters. On the other hand, partitioning of ocean water masses with similar high $\delta^{18}O$ and $\delta^{2}H$ (and thus *d-excess*) values would be more challenging to do with this analysis given the uncertainty in this particular study. Used appropriately, the continuous nature of these observations enables substantially more information to be learned about these surface water masses, especially for examining freshwater sources, than is possible from discrete sampling protocols.

2.2. Precipitation Isotopic Observations

Three precipitation events were opportunistically sampled on the USCGC Healy to compare with the seawater samples. On 22 and 23 September 2021 when the Healy was in eastern Baffin Bay, several short duration (<1 hr) snowfall events occurred from shallow convective clouds. Snowfall accumulated on ship surfaces at times, and the snow from three events were sampled during or immediately after the precipitation event and prior to any melt taking place. Sample collection occurred at 20:20 UTC on 22 September and at 8:30 and 22:30 UTC on 23 September. The snow was collected directly into 40 mL HDPE bottles and followed the same protocol for storage and analysis as the discrete underway samples described above.

2.3. Seawater Chemical and Physical Composition

Numerous other seawater properties were measured from the underway system and are used in the analyses presented in this study. In this study, we examine measurements of salinity, temperature, and fluorescence (Rolling Deck to Repository, 2021a, 2021b; see Data Availability Statement for additional details). Salinity (PSU) and temperature (°C) were measured continuously by a Seabird SBE45 thermosalinograph. Fluorescence (V) was measured continuously by a Seabird WetStar WS3S fluorometer, and calibrated to report fluorescence values as µg/L. In any temperature-salinity relationships displayed in the study, we show only the data collected during isotopic observations to provide comparative analyses.

3. Results and Discussion

The sample transect and spatial distribution of continuous $\delta^{18}O$ values from the cruise are shown in Figure 1. Corresponding maps of *d-excess*, salinity, and water temperature are presented in Figure S2 in Supporting Information S1. The $\delta^{18}O$ mean is −1.9‰ and values range between +0.6 and −6.9‰. About 40% of these measurements have $\delta^{18}O$ values less than −2‰, signaling large regions of heightened freshwater content across the cruise transit. We observe two key regions of this heightened freshwater content as marked by relatively low $\delta^{18}O$ values: (a) the Beaufort Sea and Amundsen Gulf, which contain the lowest $\delta^{18}O$ values observed; and (b) locations along the west coast of Greenland in Baffin Bay and the Labrador Sea—notably Uummannaq Fjord and

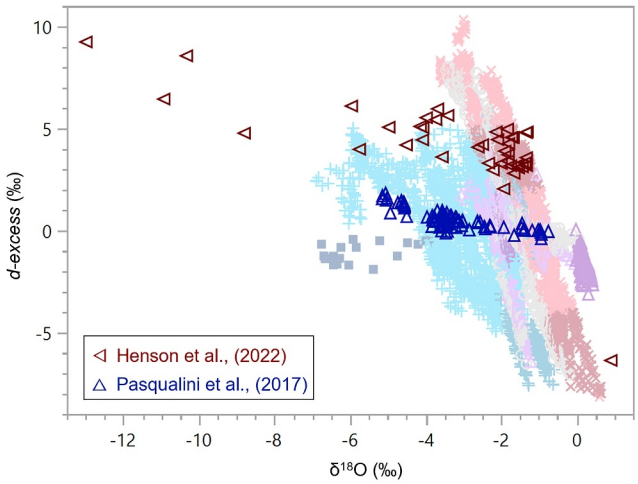

Figure 3. Seawater $\delta^{18}O$ versus *d-excess* relationships for external isotopic seawater studies, including data from Pasqualini et al. (2017) (blue △) from across the Central Arctic basin and Henson et al. (2022) (red ◁) from coastal West Greenland. External seawater isotopic data are overlying grayed-out data from this study (data points colored same as Figure 2). All data from external seawater data sets are samples collected between the surface and 10 m depth to be comparable to the continuous underway samples at ~8 m.

along the southwest Greenland coast (near Nuuk). For convenience, we include the most northeastern parts of the Labrador Sea when discussing eastern Baffin Bay.

The relationship between $\delta^{18}O$ and salinity, as anticipated, shows a broadly linear positive relationship across our data (Figure 2a). The highest freshwater content is observed in the western Arctic in the Beaufort Sea and Amundsen Gulf, with the lowest salinity and $\delta^{18}O$ values approaching 18 PSU and −7‰, respectively. In Baffin Bay, the waters with the highest freshwater context approach salinity and $\delta^{18}O$ values of 30 PSU and −4‰, respectively.

Regional variations are notably more apparent in our $\delta^{18}O$-*d-excess* data (Figure 2b), where distinct freshwater mixing relationships are observed in: (a) western Arctic (blue), (b) eastern Baffin Bay (red), and (c) western Baffin Bay/Labrador Sea (purple). This separation is not clear in the salinity-$\delta^{18}O$ plot in Figure 2a. The waters along west Greenland in eastern Baffin Bay have a strongly negative relationship between $\delta^{18}O$ and *d-excess* values, while in the other regions, there is a significantly lower negative slope between $\delta^{18}O$ and *d-excess*. The measurements near the Mackenzie River delta (dark blue squares) indicate yet further *d-excess* excursions below the other heightened freshwater regions in the western Arctic.

We focus our analyses on coastal regions where there are diverse freshwater inputs (e.g., glacial meltwater or river runoff). However, we note that in central Baffin Bay (Figure 2, gray points), the values and mixing relationships are a combination of those exhibited in the eastern and western regions of the bay.

While few studies publish both seawater $\delta^{18}O$ and $\delta^{2}H$ values, to provide additional context to this study's observations, we examine two external sets of discrete observations that have measured both $\delta^{18}O$ and $\delta^{2}H$ values (to compute *d-excess*). These two data sets include: (a) measurements in the western Arctic by Pasqualini et al. (2017) that are further described by Charette et al. (2020), and (b) measurements in eastern Baffin Bay by Henson et al. (2022) that are further described by Henson et al. (2023). Both data sets are presented on the VSMOW-SLAP scale to ensure comparability to the data set presented in this study. In Figure 3, we display the near-surface (surface to 10 m depth) isotopic observations from these two studies to compare with the isotopic observations in this study. Comparing these external data sets with the data presented in this study for similar regions, each data set reaches similar $\delta^{18}O$ maxima and correspondingly similar *d-excess* values. Moving toward fresher seawater, the waters measured by Pasqualini et al. (2017) fall along a similar $\delta^{18}O$-*d-excess* trajectory as that observed in this study. Interestingly, the freshest water in the data from Henson et al. (2022) show an isotopic divergence from the freshest waters we observed in eastern Baffin Bay. Additionally, it is important to note that there is considerably more isotopic variance observed in this study's continuous measurements as compared to that measured by the discrete sampling approaches used by Henson et al. (2022) and Pasqualini et al. (2017). We further explore key similarities and differences between these data sets in the following sections.

We note here that the focus of this analysis is on the surface water composition. This surface seawater is the water that is logistically feasible to measure with the continuous sampling methods employed in this study and is repeatable on other campaigns (e.g., Klein et al., 2024), whether on the USCGC Healy or other research vessels that typically have similar underway systems. With one instrument, these sets of measurements are only possible to do for one depth at a time, and the most convenient depth is the water continuously flowing through the underway system (sampling water from ~8 m), which is also water that is being measured for a suite of additional oceanographic measurements. This does limit our ability to assess the roles of water mass mixing, advection, and circulation across different depths. If logistically feasible, future studies may benefit from sampling at additional depths with additional analyzers and/or performing intensive discrete sampling if deeper water is being sampled. There are additional analyses that could be performed if measuring waters at different depths, but the purpose of this study is to examine a novel approach to sampling seawater continuously and show the value of including *d-excess* observations alongside other traditional physical oceanographic measurements, particularly for freshwater source delineations.

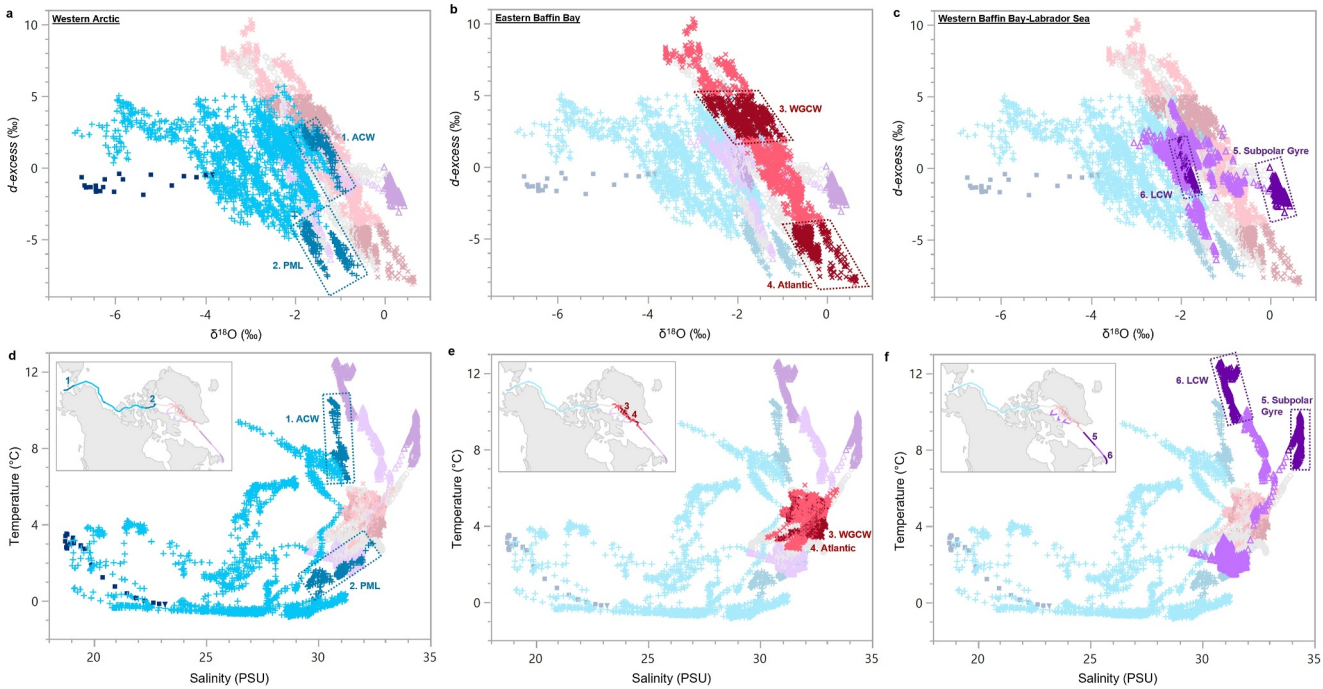

Figure 4. $\delta^{18}O$-*d-excess* mixing relationships in the three key regions covered in this cruise—(a) western Arctic (blue), (b) eastern Baffin Bay (red), and (c) western Baffin Bay-Labrador Sea (purple). Data between regions are shown in gray. Six ocean water masses are defined here, including (1) Alaska Coastal Water (ACW), (2) Polar Mixed Layer (PML), (3) West Greenland Coastal Water (WGCW), (4) Atlantic Water, (5) Subpolar Gyre Water, and (6) Labrador Coastal Water (LCW). Ocean water masses are labeled by number and displayed as dark colors of each respective region's color and outlined in dashed boxes. Water masses 3 and 4 are dispersed across eastern Baffin Bay. Temperature-salinity relationships are displayed for the same three regions—(d) western Arctic, (e) eastern Baffin Bay, and (f) western Baffin Bay-Labrador Sea—with the same coloring as the above panels. A map displaying the locations of the regional seawater measurements and locations of each ocean water mass is displayed in the small inserts in (d)–(f). All seawater data displayed at 5-min resolution.

3.1. Ocean Surface Water Mass Delineation

Across three regions—western Arctic, eastern Baffin Bay, and western Baffin Bay-Labrador Sea—we identify six distinct surface water masses based on their geographic location and data clustering in the $\delta^{18}O$ and *d-excess* values. The location and isotopic composition of these water masses are highlighted in Figures 4a–4c. Approximate isotopic values of these water masses are identified in Table 1. Corresponding water mass delineation in temperature-salinity space is shown in Figures 4d–4f.

Table 1
Ocean Water Salinity and Isotopic Values of Key Water Masses Identified in This Study, Including Alaska Coastal Water (ACW), Polar Mixed Layer (PML), West Greenland Coastal Water (WGCW), Atlantic Water (AW), Subpolar Gyre Water (SGW), and Labrador Coastal Water (LCW)

Water mass	Sal_avg	Sal_sd	Sal_max	$\delta^{18}O$_avg	$\delta^{18}O$_sd	$\delta^{18}O$_max	*d-excess*_avg	*d-excess*_sd
ACW	30.9	0.2	31.3	−1.5	0.2	−0.9	1.6	0.9
PML	30.6	0.6	32.4	−1.3	0.4	−0.6	−5.6	0.9
WGCW	32.2	0.5	32.9	−1.8	0.3	−1.0	3.5	0.7
AW	32.5	0.2	33	−0.3	0.3	0.7	−5.3	0.8
SGW	34.3	0.1	34.4	0.2	0.1	0.4	−1.8	0.5
LCW	31.2	0.2	31.7	−1.9	0.1	−1.6	0.5	0.9

Note. For salinity (PSU) and $\delta^{18}O$ (‰), the average (avg), standard deviation (sd), and maximum (max) values are shown of all the measurements identified for each water mass as identified in Figure 4. Maximum values are used for mass balance calculations. For *d-excess* (‰), the average and standard deviation are displayed.

In the western Arctic, we classify two ocean water masses (Figures 4a and 4d): (1) Alaska Coastal Water (ACW), and (2) Polar Mixed Layer (PML). Two primary data clusters in this region exist at the higher $\delta^{18}O$ limit of these waters, one with higher *d-excess* than the other. Both waters correspond with local maxima in salinity content. Given the location of ocean water mass 1, we propose that the surface waters reflect the ACW, that brings waters northward along coastal Alaska from the Pacific into the Central Arctic (Paquette & Bourke, 1974; Weingartner et al., 2005). Furthermore, our observed temperature-salinity values (Figure 4d) are similar to those previously measured (e.g., Lin et al., 2019). The isotopic composition of the ACW is similar to that measured by Pasqualini et al. (2017), where their near-surface data (≥10 m) shows a limit in a similar isotopic range (both in $\delta^{18}O$ and *d-excess*) that we define for the ACW waters (Figure 4a). The location of the second high-$\delta^{18}O$ end member was across the eastern entrance to Lancaster Sound from Baffin Bay, likely influenced by the southward-flowing Nares Strait current as it flows into Baffin Bay. We define this water mass as PML, consisting predominately of waters exiting the Beaufort Gyre (Rudels et al., 1996).

Along the Greenland coastline in eastern Baffin Bay, we classify two ocean water masses (Figures 4b and 4e): (3) West Greenland Coastal Water (WGCW), and (4) Atlantic Water (AW). The WGCW is defined by a primary data cluster that exists along this trajectory with *d-excess* values between 3 and 5‰, containing the mode of the distribution of all data in this region (>30% of regional data fall within this small isotopic range). These waters are spatially dispersed across most of the eastern Baffin Bay region covered by the cruise. The isotopic composition of the WGCW is very similar to the isotopic end member observed by prior isotopic measurements by Henson et al. (2022) in this region, where their near-surface data (≥10 m) shows a clear limit in this same isotopic range (both in $\delta^{18}O$ and *d-excess*) we define for the WGCW waters (Figure 4b). The location and physical parameters are consistent with other studies of the WGCW (Carroll et al., 2018; Curry et al., 2014; Rysgaard et al., 2020). We classify a second water mass as AW defined by the highest $\delta^{18}O$ and lowest *d-excess* values. These two ocean water masses along coastal West Greenland overlap considerably in water temperature-salinity space (Figure 4e), but they have very different isotopic signatures, which requires this second water mass classification. Without analyzing their $\delta^{18}O$-*d-excess* composition, these waters would not likely be classified as distinct water masses. The measurements made by Henson et al. (2022) also show one anomalous low *d-excess* observation in their near-surface samples that is consistent with the AW defined in this study.

Finally, in western Baffin Bay-Labrador Sea we classify two additional ocean water masses (Figures 4c and 4f): (5) Subpolar Gyre Water (SGW), and (6) Labrador Coastal Water (LCW). As perhaps the clearest isotopic composition of any of these ocean water masses, the cluster of data points around $\delta^{18}O$ and *d-excess* values near 0‰ (Figure 4c) represent a distinct surface water mass, and given the location we classify this as the SGW (Reverdin et al., 2003). A second major data cluster exists along the Canadian Coastline near Labrador, which we classify as LCW. The waters further north in this region along Baffin Island also show a similar isotopic composition, so we could also consider these waters to be, in part, the surface waters in Baffin Island Current that ultimately flow southward becoming part of the LCW. When examining these waters in temperature-salinity space (Figure 4f), these data cluster as much colder but similar salinity water to the LCW, which would be consistent with these upstream waters being a part of the Baffin Island Current. These observations also show that this surface water mass is comprised of a significant amount of freshwater where approximate $\delta^{18}O$ and salinity are −2‰ and 31 PSU, respectively.

3.2. Partitioning Freshwater Sources and Mixing Relationships

As described previously, clear and different mixing relationships exist between ocean water and freshwater sources. In this section, we explore the roles of river runoff, precipitation, glacial meltwater, and sea ice meltwater as potential sources of freshwater to the regions sampled during this cruise. In particular, we focus on identifying the key drivers of the freshwater sources that lead to the significantly different $\delta^{18}O$-*d-excess* relationships between those observed in Eastern Baffin Bay and the Western Arctic, as well as the variations within the Western Arctic (i.e., the "Mackenzie River" observations from other Western Arctic measurements). We focus on the most pertinent sets of measurements to the freshwater sources contributing to the seawater measured on this study's cruise, but we share a comprehensive set of relevant freshwater end member data in Table S1.

In the following sections, we will demonstrate that a key to delineating these freshwater sources from one another is their unique *d*-excess values. While these freshwater sources typically have similarly lower $\delta^{18}O$ values (the exception being sea ice meltwater; discussed in Section 3.2.3), their *d*-excess values vary considerably between

sources. We utilize a suite of isotopic measurements from across the Arctic to inform and ultimately quantify the different freshwater sources driving the mixing relationships observed in this cruise.

3.2.1. Meteoric Water

The primary source of freshwater across much of this cruise is from meteoric water (MW)—precipitation and river runoff. We distinguish these meteoric inputs from glacially-derived freshwater, which is described in 3.2.2 below. This MW includes both precipitation that falls directly over the ocean and that which occurs over land and enters the Arctic seas via surface runoff. Measurements of the isotopic composition of precipitation falling over the ocean are relatively limited, however we were fortunate to sample three snowfall events in Eastern Baffin Bay during the 2021 Healy cruise. Aside from the events sampled on the cruise, we use prior land-based measurements to inform the precipitation isotopic composition of this freshwater source (Kopec et al., 2016; Putman et al., 2017), where these observations represent both precipitation directly onto the ocean surface and runoff from surrounding terrestrial regions. In this study, we focus on precipitation measurements during the time of the cruise (i.e., August, September, and/or October), computing the arithmetic average of precipitation samples for the given month over the time period of the respective measurement period. The largest deliveries of freshwater from rivers are the Yukon and Mackenzie Rivers, which have been sampled extensively for their isotopic composition (e.g., Gibson et al., 2020; The Arctic Great Rivers Observatory, 2024; Yi et al., 2010). We utilize observations from the Arctic Great Rivers Observatory (ArcticGRO; The Arctic Great Rivers Observatory, 2024) where the Yukon and Mackenzie Rivers are sampled near their respective mouths to determine flow-weighted isotopic values of this freshwater input. For these ArcticGRO observations, we compute the flow-weighted and arithmetic average isotopic composition for the entire period of measurements (2003–2021) and the flow-weighted average for the measurements in the year prior to (and including) the cruise (October 2020 to September 2021). We consider the arithmetic mean useful here because there are limited samples each year (typically $n = 6$ to 8 samples), so the flow weighted mean is not necessarily more representative of the input over time. For these two rivers, these computations yield relatively similar isotopic values, but we show all three values to ensure representativeness of this freshwater end member is captured. The isotopic values of this suite of freshwater end members are shown in Table S1 for the time periods relevant to this cruise.

To identify the specific freshwater source driving the mixing relationships in each region, we display the most pertinent freshwater end members in Figure 5a accompanying the seawater isotopic observations. First, we explore the key freshwater drivers in the Western Arctic. In Figure 5a, it can be seen that freshwater from the Yukon River and precipitation from Utqiagvik and around the Canadian Archipelago fall along a similarly sloped δ^{18}O-*d-excess* relationship that fits Western Arctic seawater data where the freshest (lowest δ^{18}O) observations extend directly toward these freshwater end members. It is clear that these MW sources drive the primary freshwater relationships across this region. The near-surface seawater measured by Pasqualini et al. (2017) exhibits a very similar mixing relationship, as the waters with the most negative δ^{18}O values extend directly toward these same freshwater end members (Figure 5b).

As mentioned previously, seawater measurements from near the Mackenzie River mouth have markedly lower *d-excess* than waters with similar δ^{18}O values in the surrounding region (e.g., Yukon River), where the isotopic excursion occurred over a period of less than 2 hr. These lower *d-excess* values suggest the Mackenzie River waters were distinct from other freshwater inputs (Figure 5a). For example, Gibson et al. (2020) show that Mackenzie River region contains many of the lowest flow-weighted *d-excess* values compared to other northern Canadian Rivers. The large Mackenzie watershed has potential for significant evaporation to take place, which would produce waters with relatively low *d-excess* (*d-excess* = 0.6‰; Table S1) as compared to other regional meteoric contributions. The Mackenzie River watershed also contains large lakes and wetland areas where water is stored in the system for longer than other nearby river systems and are thus further affected by evaporation, which contributes to the lower *d-excess* values (Lesack & Marsh, 2010; Yi et al., 2012). The isotopic end member of the Mackenzie River may differ at other times of the year given differences in discharge and amount of evaporation of the river water (The Arctic Great Rivers Observatory, 2024; Yi et al., 2010), but the timing of our measurements enabled clear identification. It should also be noted that this unique Mackenzie River signature is not visible in the data when viewed in salinity-δ^{18}O space (Figure 2a) or temperature-salinity space (Figure 3d), where it overlaps directly with other nearby data. In other words, the freshening signal by the Mackenzie or Yukon Rivers display the same in temperature-salinity space, yet display with differentiable signals in δ^{18}O-*d-*

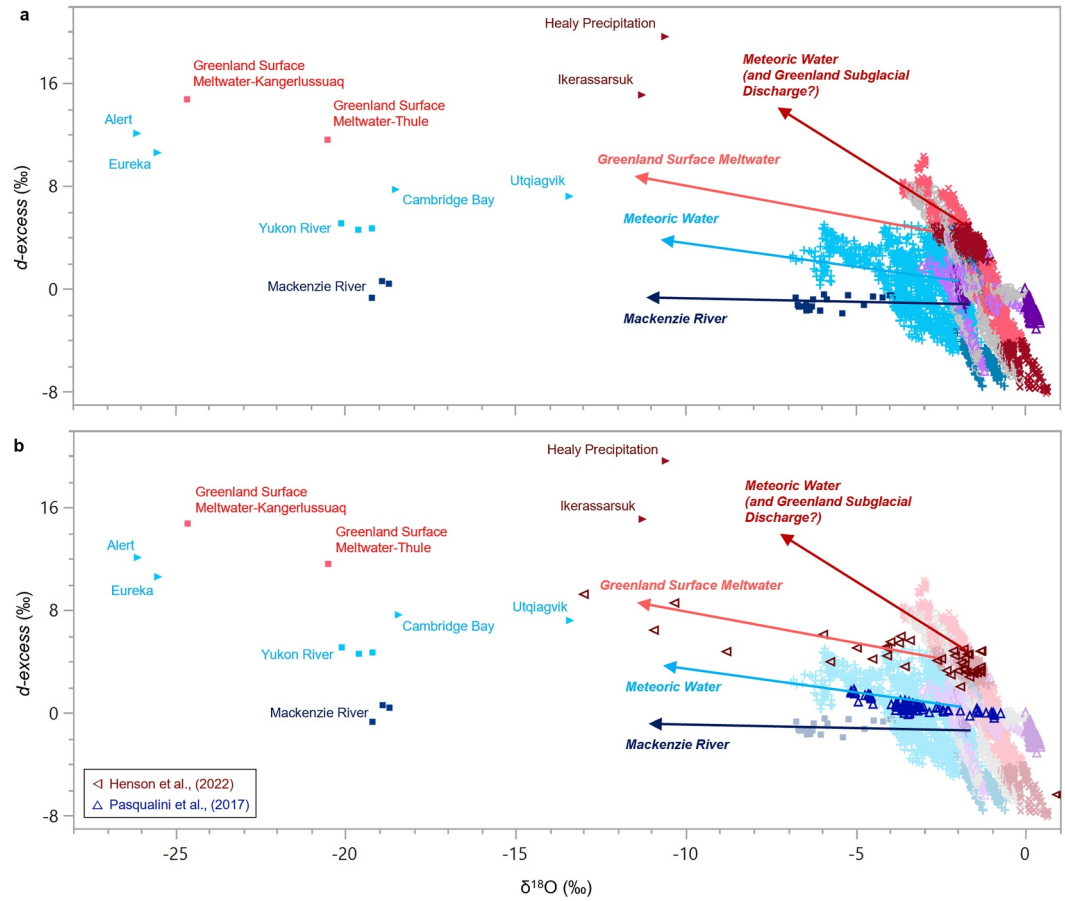

Figure 5. (a) δ^{18}O-*d-excess* freshwater mixing model between the seawater isotopic measurements (as colored in Figures 2 and 4) with freshwater isotopic end members (see Table S1 for additional details on freshwater sources). Precipitation measurements are displayed as ► and river inputs as ■ in the color of the respective mixing relationships for each region. Precipitation values are used for the month when the United States Coast Guard Cutter was nearest the given region, including August for Utqiagvik, September for Alert, Cambridge Bay, and Eureka, and October for Ikerasaarsuk. The flow weighted (for 2003–2021 and October 2020 to September 2021) and arithmetic means for the Yukon and Mackenzie Rivers are displayed. (b) Same δ^{18}O-*d-excess* freshwater mixing model as (a) but displaying the external seawater isotopic data sets overlying the seawater data presented in this study. Data from external studies by Pasqualini et al. (2017) (blue △) from across the Central Arctic basin and Henson et al. (2022) (red ◁) from West Greenland fjords are shown overlaying grayed-out data from this study. Arrows depicting direction of extension by freshwater end members are identical in each panel.

excess space. Using *d-excess* measurements facilitates detailed partitioning and tracing of such specific water sources.

In Eastern Baffin Bay, to produce the observed mixing relationship in Figure 2b, the freshwater end member(s) must have relatively high δ^{18}O and *d-excess* values, where these *d-excess* values are significantly higher than those in the western Arctic. Each of the three precipitation samples collected on the Healy in this region had an isotopic composition that would reasonably represent the freshwater end member of the eastern Baffin Bay mixing line (Figure 5a)—that is, relatively high δ^{18}O and *d-excess* values compared to other known freshwater sources—with an average $\delta^{18}O = -10.6‰$ and *d-excess* = 19.6‰ ($n = 3$; Table S1). This anomalous combination of high δ^{18}O and *d-excess* values has also been observed from daily precipitation in October (2011–2014) in Ikerasaarsuk in coastal West Greenland (Table S1), suggesting the type of precipitation events observed during the cruise are representative of typical precipitation during this time of year in Eastern Baffin Bay. Elsewhere in the Arctic, autumn precipitation often has high *d-excess* values, but much more negative δ^{18}O values (Table S1; Kopec et al., 2016; Putman et al., 2017), so it appears this particular combination of high δ^{18}O and high *d-excess* values is unique to the Baffin Bay and/or West Greenland system. Based on these isotopic observations, this local precipitation and any subsequent runoff drives the freshwater mixing relationship in this region. The amount of

precipitation produced during these events is, however, rather low overall. The ClimateBasis Disko site on Disko Island operated by the Greenland Ecosystem Monitoring program only measured 3.7 mm of precipitation from 10 September through 7 October 2021 (See Data Availability Statement for more details). ERA5 reanalysis (Hersbach et al., 2023) shows considerably higher precipitation in some regions of Baffin Bay (up to 10 cm in September; Figure S3 in Supporting Information S1), but still rather small quantities. It is likely that this precipitation is a key driver of the δ^{18}O-*d-excess* mixing line, but probably does not account for the totality of the freshwater along this mixing line. We explore the potential roles of glacial and sea ice meltwater in the subsequent sections.

In the western Baffin Bay-Labrador Sea, we observe more limited roles of freshwater in the mixing relationships. As noted above, the LCW is the primary export of water from this region, and has among the freshest surface water in this region. There are slightly lower δ^{18}O and/or higher *d-excess* values in some regions that indicate similar precipitation and runoff sources as described in the other regions, but with more limited influence. It is likely similar precipitation events as in Eastern Baffin Bay led to the heightened *d-excess* values, while runoff from Baffin Island and other regions of the eastern Canadian Archipelago drive the lower δ^{18}O values, which is consistent with river isotopic content observed by Gibson et al. (2020). While not a focus of this study, we also note that the waters in Central Baffin Bay exhibit properties and mixing relationships that are a combination of those observed in the eastern and western portions of the bay. The δ^{18}O-*d-excess* and temperature-salinity relationships for Central Baffin Bay are displayed in Figure S4 in Supporting Information S1.

3.2.2. Greenland Glacial Meltwater

In this section we focus on the roles of meltwater sourced from the Greenland Ice Sheet and its outlet glaciers as a potential source of freshwater to the Eastern Baffin Bay section of this cruise. As noted in the prior section, it seems unlikely that precipitation and runoff account for the totality of the freshwater inputs to this region. Given the large potential source of freshwater from ice in Greenland, it is plausible that meltwater would be a significant contributor to the seawater sampled during this cruise.

As described previously, the freshwater end member that drives the seawater mixing line observed in Eastern Baffin Bay requires having both a relatively high δ^{18}O and *d-excess* composition (Figure 5a). Prior measurements of proglacial rivers and meltwater on the surface of the Greenland Ice Sheet from around West Greenland (Csank et al., 2019; Kopec et al., 2018) show that these waters have a combination of too low of δ^{18}O values and not high enough *d-excess* values (Table S1) to reasonably represent this end member (Figure 5). It is surely the case this freshwater is some small proportion of the seawater measured (<10%), but our observations do not support there being significant contributions of surface inputs of meltwater (e.g., proglacial rivers) to this region during our time of study. Surface inputs of meltwater clearly account for a significant proportion of coastal Greenland seawater in other studies (e.g., Henson et al., 2023), where the Henson et al. (2022) isotopic data show a clear extension toward the Greenland meltwater end members (Figure 5b). However, these isotopic excursions are not observed in this study. It is reasonable to assume that there is limited influence of surface inputs of meltwater during this cruise because the melt period had essentially ended prior to the USCGC Healy entering Baffin Bay; surface melt extent fell below 10,000 km^2 on 4 September 2021 as shown in the National Snow and Ice Data Center's Greenland Daily Melt extent data set (based on Mote (2014) and Mote and Anderson (1995)). We reiterate that it is likely that there is some amount of surface derived meltwater in the Eastern Baffin Bay system, and that it might cause some of the variance in the δ^{18}O-*d-excess* relationship, but it is not observed to be a dominant source of freshwater in this study by this method.

While it seems likely that local precipitation (and subsequent runoff) is driving the freshwater mixing relationships in Eastern Baffin Bay during the time of this cruise, the generally small quantities of precipitation in the observed events suggests the possibility of an additional source of freshwater beyond this local precipitation input. With the observed lack of surface inputs of meltwater, we suggest the possibility of significant subglacial discharge of basal meltwater from marine-terminating glaciers. There is significant subglacial discharge of basal meltwater from marine-terminating glaciers directly into this system in autumn (and subsequent months), and it is potentially a significant source of this freshwater observed in Baffin Bay (Bendtsen et al., 2015; Mortensen et al., 2013). Direct isotopic measurements of this subglacial discharge have not been made but it is plausible the *d-excess* could be higher than expected for other components of the glacial melt system, especially when the ocean water is interacting directly with the ice (Chauché et al., 2014), as there are many unknown processes at

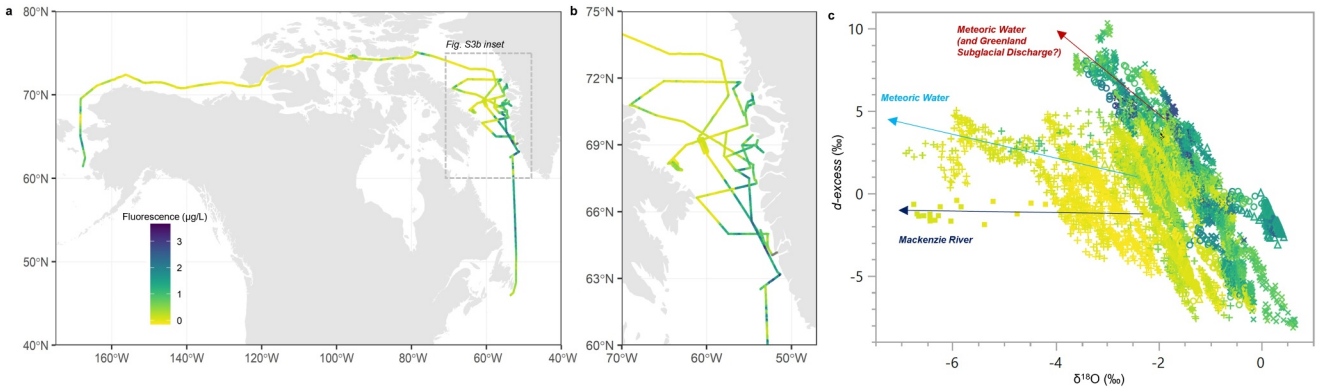

Figure 6. (a) Map of entire United States Coast Guard Cutter Healy cruise track and (b) zoom in of transects in Baffin Bay and Labrador Sea colored by 5-min average fluorescence values (µg/L). (c) 5-Min average $\delta^{18}O$ versus *d-excess* colored by fluorescence. Data points displayed as the same symbols as in Figure 2. Key freshwater mixing relationships from Figure 5 displayed.

work where isotopic fractionation could take place. More investigation is needed to identify the isotopic signals of this flux and the exact role of this freshwater in this marine system, but given the potential need for an additional freshwater flux and the biologic response that is described next, it is at least a potential unknown flux that would be consistent with the observations.

Significant subglacial discharge from marine-terminating glaciers would also be consistent with measures of biological productivity (Figure 6), where regions of relatively high productivity are associated with heightened freshwater, supporting the mechanism where subglacial discharge directly into the ocean entrains nutrients at depth and brings them to the surface to enhance productivity (Hopwood et al., 2018; Kanna et al., 2018; Meire et al., 2017). If this freshwater were only sourced by precipitation and surface runoff, this freshwater would remain near the ocean surface and further limit near-surface nutrient availability (e.g., Carmack et al., 2016; Farmer et al., 2021; Fu et al., 2020). This effect is seen in the other regions covered by the cruise, whereas along coastal West Greenland heightened productivity corresponds, at times, with higher freshwater content. It is quite possible much of the heightened productivity is driven by other causes of upwelling, but the subglacial discharge hypothesis is at least plausible given the productivity levels reaching their highest values even when freshwater content is also at its highest level. This is particularly the case in Uummannaq Fjord where the greatest regional freshwater content (i.e., lowest $\delta^{18}O$ and salinity values) is observed in conjunction with heightened productivity levels (Figure 6). We postulate this hypothesis from the data presented here, as it would be consistent with prior observations of these systems (Hopwood et al., 2018; Kanna et al., 2018; Meire et al., 2017) and significant subglacial discharge could account for the potential need for a second substantial freshwater source. Therefore, we consider the primary freshwater sources in eastern Baffin Bay at the time of the cruise to be local precipitation and runoff and a potential significant secondary contribution from subglacial meltwater. Subglacial discharge as a freshwater source would be most prominent in the fjords containing these marine terminating glaciers (e.g., Uummannaq Fjord), but some of this water could be circulated to broader regions of eastern Baffin Bay.

3.2.3. Sea Ice Meltwater

Given the location and timing of this cruise, it is plausible that meltwater derived from sea ice comprises some significant proportion of the freshwater measured. It is, however, more difficult to tease out these contributions in $\delta^{18}O$-*d-excess* space given the isotopic composition of sea ice that is much more similar to the seawater than the other freshwater sources discussed in this study. For example, Tian et al. (2018) show from a suite of sea ice observations in the Beaufort and Chukchi Seas that the average $\delta^{18}O = -3.4 \pm 2.9‰$ (mean ± standard deviation) and *d-excess* = 2.0 ± 1.5‰; the median sea ice values are $\delta^{18}O = -2.4‰$ and *d-excess* = 1.6‰. These observations are similar to, but slightly more negative than, $\delta^{18}O$ values in other prior studies of Arctic sea ice where observations of this end member range between +1 and −3‰ (e.g., Eicken et al., 2002; Forryan et al., 2019; Sutherland et al., 2009; Yamamoto-Kawai et al., 2009); *d-excess* (or simply $\delta^{2}H$) values are not typically shown in these studies. At least some of the samples in the Tian et al. (2018) study contain MW that has melted and refrozen, so these values are perhaps not ideal for a pure sea ice end member, but these measurements can still

inform the meltwater signal where *d-excess* observations are quite limited. For quantifying the sea ice meltwater component (Section 3.2.4), we use the $\delta^{18}O$ values presented by Eicken et al. (2002) for a similar geographic region and that have excluded samples of any layers infiltrated by MW, where $\delta^{18}O = -1.9 \pm 0.5‰$ (mean ± standard deviation).

Unlike the meteoric waters, the isotopic composition of the sea ice meltwater is not sufficiently different isotopically to the surrounding seawater to effectively tease out this signal using the isotopic values alone, at least for the isotopic ranges observed in this study. Pairing these isotopic measurements with salinity observations, however, can allow one to assess the contributions of sea ice (Eicken et al., 2002; Sutherland et al., 2009; Yamamoto-Kawai et al., 2009). Eicken et al. (2002) show the average salinity value is 4.5 ± 2.6‰, consistent with other studies (Sutherland et al., 2009; Yamamoto-Kawai et al., 2009). If sea ice melt is a significant freshwater contributor to seawater without other sources of heightened freshwater content (i.e., seawater salinity >30 PSU and $\delta^{18}O > -1‰$), the signal would be seen as a slight or no change to $\delta^{18}O$ values and a significant change to lower salinity values. In salinity-$\delta^{18}O$ space, locations where sea ice is a primary source of freshwater would show significant excursions from the typical salinity-$\delta^{18}O$ mixing line to values above that line as driven by the relatively larger salinity changes (Forryan et al., 2019; Sutherland et al., 2009).

We examine the salinity-$\delta^{18}O$ relationships (Figure 2a) to see if a sea ice signal is observed. The salinity-$\delta^{18}O$ relationships are also displayed (Figure S5 in Supporting Information S1) alongside key freshwater end members (as in Figure 5) to show additional context of these mixing relationships. The observed salinity-$\delta^{18}O$ relationship across this cruise has a strong correlation throughout the cruise, with limited excursions from the primary mixing relationships. The region most likely to be affected by sea ice meltwater in this study is the waters within the Canadian Archipelago. This region is the only area of the cruise with direct interaction with sea ice, especially in Melville Sound and Parry Channel. As seen in the Western Arctic seawater salinity-$\delta^{18}O$ data (Figure 2a, Figure S5a in Supporting Information S1), there are some data points that extend to lower salinity values than the primary mixing line. It is likely there are regions in the Western Arctic where sea ice meltwater comprises a significant proportion of the freshwater content. However, these proportions are relatively small compared with the MW contributions (e.g., Mackenzie River). We explore this quantitively in Section 3.2.4.

On the other hand, in eastern Baffin Bay, there is little to no residual freshwater from sea ice melt at the time of this cruise. In this region, the lowest salinity values correspond to the lowest $\delta^{18}O$ values (Figure 2a, Figure S5b in Supporting Information S1), where the slope of the salinity-$\delta^{18}O$ is higher than that of the full data set. The freshest waters in this region are pulled in the opposite direction (below) on the expected mixing line for sea ice melt contributions (i.e., to low $\delta^{18}O$ values, not relatively high ones). It is likely that any sea ice meltwater has largely circulated out of the region by the time of these measurements. Sea ice had largely melted from the entire coastal Greenland region by July, and Baffin Bay was essentially ice free by 1 August (data from Multisensor Analyzed Sea Ice Extent—Northern Hemisphere, Version 1—U.S. National Ice Center and National Snow and Ice Data Center, 2010). Sea ice meltwater may play a role in driving some of the variance around the salinity-$\delta^{18}O$ line in the different regions of the cruise, but, unlike the MW, it does not appear that sea ice meltwater is a primary driver of the large freshwater proportions observed in the seawater.

Sea ice freeze up could also play a role in altering the freshwater composition of the observed seawater. However, sea ice growth did not begin by the time the USCGC Healy passed through the respective regions covered by this study (U.S. National Ice Center and National Snow and Ice Data Center, 2010). Even in the later stages of the cruise in early-October when sea ice growth was underway in some regions of the Arctic, sea ice growth had not yet begun in any parts of Baffin Bay.

3.2.4. Quantifying Freshwater Contributions

In the above sections, we qualitatively explore how these isotopic observations can be used to identify distinct freshwater sources from one another. Here, we quantitatively examine the freshwater proportions across the regions covered in this study using the seawater isotopic and salinity values, ocean water mass end members determined in Section 3.1, and the freshwater end members described throughout Section 3.2. We focus our efforts on the Western Arctic and Baffin Bay systems where freshwater sources are constrained as described in the analyses above.

In the Western Arctic, the primary freshwater sources include MW and sea ice meltwater. As has been done in numerous prior studies (e.g., Alkire et al., 2017; Bauch et al., 1995; Cooper et al., 2022; Sutherland et al., 2009; Yamamoto-Kawai et al., 2008), we use the combination of seawater isotopic and salinity values to determine the fraction of respective sources for any given data point. Because the combination of $\delta^{18}O$ and *d-excess* values for sea ice meltwater is contained within the primary data cluster of Western Arctic data, we utilize $\delta^{18}O$ and salinity values to first determine the fraction of sea ice meltwater and MW. We then use the *d-excess* values to tease apart the meteoric waters derived from the Mackenzie River. To determine the fraction (f) of MW, sea ice melt water (SIM), and oceanic water (OW), we use the following set of three mass balance equations based on $\delta^{18}O$ and salinity (S) data.

$$f_{MW} + f_{SIM} + f_{OW} = 1 \quad (1)$$

$$\delta^{18}O_{MW} f_{MW} + \delta^{18}O_{SIM} f_{SIM} + \delta^{18}O_{OW} f_{OW} = \delta^{18}O_{Obs} \quad (2)$$

$$S_{MW} f_{MW} + S_{SIM} f_{SIM} + S_{OW} f_{OW} = S_{Obs} \quad (3)$$

Using the $\delta^{18}O$ and salinity end members for respective water masses and the observed (Obs) $\delta^{18}O$ and salinity values throughout the cruise, the fraction of each water mass can be determined for each data point. For MW inputs, we use the average of flow-weighted Mackenzie and Yukon River $\delta^{18}O$ values ($-19.2‰$) and assume salinity = 0 PSU. For sea ice meltwater, we use the mean values measured by Eicken et al. (2002) for their sea ice cores where $\delta^{18}O = -1.9‰$ and salinity = 4.5 PSU. For the ocean water end members, we use the maximum value observed in the Western Arctic where $\delta^{18}O = -0.6‰$ and salinity = 32.4 PSU (Table 1).

Using the three mass balance equations and respective end members and observations, we compute the fraction of water masses across the Western Arctic (Figure 7). Contributions of meteoric waters are seen in Figure 7a, showing heightened regions of freshwater across the Western Arctic, with highest concentrations in the Beaufort Sea. Meteoric water comprises up to 33.4% of the measured seawater, with a mean of 11.8% ± 5.9% (mean ± 1 standard deviation; median is 10.8%). Sea ice meltwater is also a contributor to the observed seawater across the Western Arctic, but at a significantly smaller proportion, on average, than the meteoric contributions. The mean sea ice meltwater is 3.6% ± 4.5% (median is 1.4%), and a maximum of 20%. The areas of highest sea ice meltwater are in the western Canadian Archipelago—where sea ice was present on this cruise—as well as in the Beaufort Sea.

We utilize the *d-excess* observations to further delineate meteoric waters across the Western Arctic. From the observed *d-excess* values, we partition the fraction of MW as a percentage of Mackenzie or other meteoric sources (e.g., Yukon River). We use the ArcticGRO flow-weighted *d-excess* values of the Mackenzie and Yukon Rivers as the two primary end members, making the assumption that the Yukon River is representative of non-Mackenzie meteoric waters, which is consistent with the freshwater mixing line observed in Figure 5a. If observed *d-excess* values are less than the Mackenzie end member, we assume that the meteoric contribution is 100% from the Mackenzie, and if the observed *d-excess* values are greater than the Yukon River end member, we assume the meteoric contribution is 100% from non-Mackenzie meteoric waters.

The Mackenzie River proportions in the observed seawater are displayed in Figure 7c. The difference between the total MW (Figure 7a) and the Mackenzie River (Figure 7c) proportions is the non-Mackenzie River contribution to the total seawater. As expected, it is observed that the highest Mackenzie River water content is nearest the Mackenzie River delta, as well as other heightened regions to the east into the Canadian Archipelago. There may be additional inputs with similarly low *d-excess* inputs where Mackenzie-like water from other river basins yields anomalously high Mackenzie River proportions. For example, this is likely the case along the coast of Alaska near the Bering Strait region where other low *d*-excess freshwaters likely comprise much or all of what is shown as Mackenzie water in Figure 8c. That said, in much of the rest of the Western Arctic, this additional classification of freshwater using *d-excess* measurements does allow for Mackenzie River water to be effectively delineated from other regional meteoric waters.

In Baffin Bay and the northern Labrador Sea, the primary freshwater source is identified to be local non-glacial MW (precipitation and runoff). As described in Section 3.2.3, sea ice meltwater is shown to have little to no influence on the water in this region at the time of the cruise given the observed $\delta^{18}O$-salinity relationships. For the purpose of these simple mass balance computations, we assume zero sea ice meltwater in these waters, and

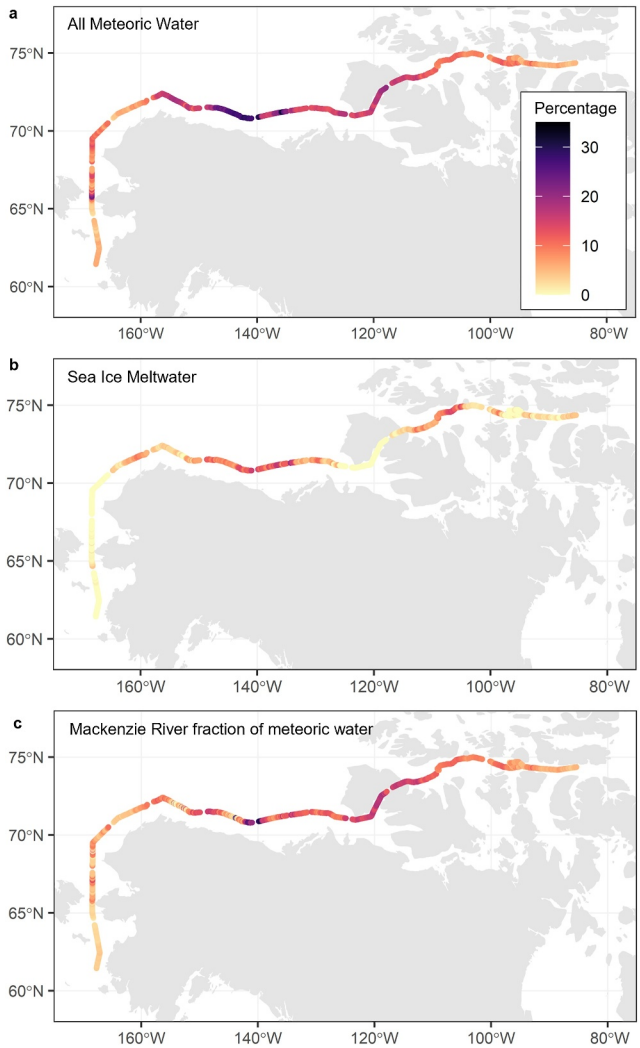

Figure 7. Freshwater proportions based on water mass balance computations for Western Arctic, including (a) proportion of meteoric water, (b) proportion of sea ice meltwater, and (c) proportion of Mackenzie River water. See Section 3.2.4 for additional details.

only consider the mixture of the primary ocean water mass and local precipitation/runoff. With mixing between only two end members, Equation 2 or 3 can each be solved on their own with Equation 1 for the respective fractions. For the ocean water end member, we use the maximum $\delta^{18}O$ and salinity values observed in the WGCW (Table 1), the dominant water mass in this region. For simplicity, we assume that for any waters in this region with $\delta^{18}O$ and salinity values greater than that of the maximum WGCW values the given sample is 100% ocean water (a mixture of WGCW and AW). For the freshwater end member, we consider the average of September and October precipitation observations at Ikerassarsuk ($\delta^{18}O = -12.3‰$) to be broadly representative of this regional fresh end member given the longer and much larger precipitation data set at this site compared with the few precipitation events captured directly on the Healy (Ikerassarsuk $n = 87$ compared to Healy $n = 3$).

We show the MW composition across Baffin Bay as determined from $\delta^{18}O$ values in Figure 8. Meteoric water composition determined by salinity is shown in Figure S6 in Supporting Information S1. The highest concentrations of MW are observed across Uummannaq Fjord, as well as in smaller clusters along coastal West Greenland and Baffin Island. Regions of heightened freshwater as computed by salinity yield similar spatial results. As determined by $\delta^{18}O$, the mean meteoric contribution is 5.8% ± 5.1% (median is 5.9%), and a maximum of 24.1%. Using salinity measurements to compute the meteoric contribution, smaller proportions are yielded where the mean contribution is 3.0% ± 2.4% (median is 2.9%), and a maximum of 10.2%. This discrepancy could be the result of a missing or different freshwater end member. Using the collected Healy precipitation to represent the fresh end member, the results of the freshwater proportions as determined by $\delta^{18}O$ would only make the discrepancy larger where higher MW proportions would be computed. As mentioned earlier, it is plausible subglacial discharge could be a significant freshwater component, particularly in Uummannaq Fjord. Alternatively, other meteoric sources with different isotopic compositions could be more representative of the broader freshwater component across Baffin Bay than the one used here. If that meteoric source had $\delta^{18}O$ value similar to that of other regions (e.g., $\delta^{18}O = -20‰$), the freshwater proportion based on the $\delta^{18}O$ calculation would yield similar results similar to that of the salinity-based calculations. Regardless of approach, while there are areas of heightened freshwater content, it is evident that the surface waters across the Western Arctic region of this cruise had higher freshwater content than the waters in Baffin Bay and the northern Labrador Sea.

Future versions of the freshwater proportion calculations can benefit from additional multi-end member mixing models with additional variables (e.g., nutrients) to further partition the freshwater quantities in a given water mass. We also note that these freshwater estimates can vary considerably depending on mixing, advection, upwelling, and other processes, but these calculations give rough estimates based on available information. Particularly for confirming the presence of subglacial discharge contributing to the freshwater content, or further constraining the absolute values of these other freshwater proportions in these given water masses, more comprehensive studies across a range of depths in addition to the surface measurements would be needed.

4. Conclusions

In this study, we show that important insights into the partitioning of distinct freshwater sources and delineation of surface ocean water masses can be obtained by examining the seawater $\delta^{18}O$-*d-excess* relationships. Delineating these same surface water masses and mixing relationships would not have been feasible from temperature-salinity or salinity-$\delta^{18}O$ measurements alone. In particular, seawater *d-excess* measurements offer a useful tool to identify distinct freshwater sources and trace their transport through the ocean, though it is critical that these systems

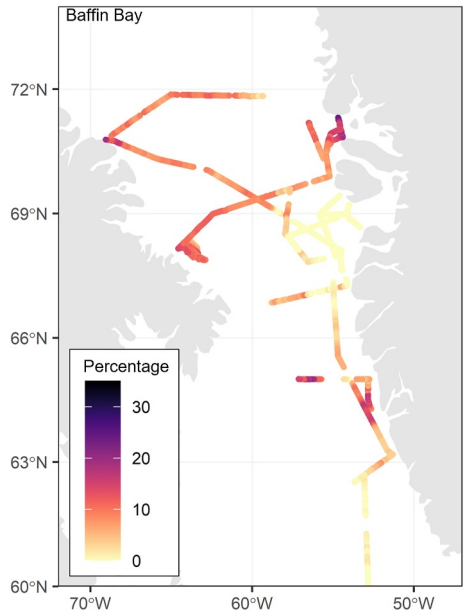

Figure 8. Meteoric water proportions based on water mass balance computations for Baffin Bay. See Section 3.2.4 for additional details.

contain a high amount of freshwater, and that the freshwater sources have diverse isotopic signatures. This is the case in this Arctic system, where we observed freshwater content up to 33% derived from meteoric sources and up to 20% from sea ice meltwater. We further delineated the unique signals of the Mackenzie from the Yukon River and other local precipitation inputs. While not observed directly in this study, we show that in the study by Henson et al. (2023), glacial meltwater inputs can be identified in seawater samples.

The continuous measurements presented in this study also enable a more detailed examination of high-definition mixing relationships and capture a greater range of variability that exists in ocean water than would be observed with discrete samples. Our continuous measurements allowed for the identification of the Mackenzie River waters that the Healy transited through in less than 2 hr, and the *d-excess* measurements enable the delineation of this particular freshwater source from other regional sources. Similarly, along coastal West Greenland, two distinct surface water masses were identified from the isotopic measurements that would otherwise be considered the same in temperature-salinity space.

The nature of continuous measurements also enables a large study area to be surveyed in a detailed manner and within a short temporal scale that would otherwise be logistically infeasible with discrete sampling techniques. In this cruise, 30° of latitude and 115° of longitude were covered within a 40-day window. While freshwater delineations might be possible with detailed sampling, using isotopic observations to compliment standard physical oceanographic measurements (e.g., Dubinina et al., 2019; Macdonald et al., 1995), regional coverage during a single cruise would be highly challenging.

Given the wide spatial coverage of this cruise, the observations and mechanisms described here can be applied to other regions of the Arctic with similar settings. For example, the freshwater inputs along the Siberian coast (e.g., The Arctic Great Rivers Observatory, 2024) would likely cause similar isotopic divergences in the seawater as we observed in coastal Alaska. However, the observations from this cruise are not necessarily temporally representative. The isotopic signals of the end members identified here (both ocean water masses and freshwater sources) may experience temporal cycles (e.g., annual) or will evolve over time, so continuing to measure these water masses is important. For example, the isotopic signal of the Mackenzie River changes some throughout the hydrological year (Gibson et al., 2020; The Arctic Great Rivers Observatory, 2024; Yi et al., 2010), so interpreting its influence in any future observations will require additional monitoring of the riverine fluxes and flow dynamics. Resampling these same regions for their isotopic composition in the future and at different times of the year will add significant new insight into these freshwater fluxes and their impacts.

Finally, we note that it is important to consider the wide range of seawater isotopic values observed in this study, which is consistent with other recent studies of Arctic seawater (e.g., Bonne et al., 2019; Klein et al., 2024; Mellat et al., 2024). In many studies, particularly for large modeling efforts, the ocean water isotopic composition is informed with coarse, lower variance gridded data (e.g., the data presented by LeGrande & Schmidt, 2006) or simply assumed to have composition of $\delta^{18}O = \delta^{2}H = d\text{-}excess = 0‰$ or a small range of near-zero values (e.g., Brady et al., 2019; Lee et al., 2007; Mathieu et al., 2002; Nusbaumer et al., 2017). There are numerous rational reasons to make these assumptions (e.g., computational limitations in modeling exercises), and those assumptions may be appropriate for many analyses on certain spatial and/or temporal scales, but for other analyses it may be important to consider the potential for a wider range of seawater isotopic compositions (especially *d-excess*). This is particularly true for studies considering the evaporative fluxes from Arctic Ocean waters where such isotopic variations in the source ocean waters would significantly impact the corresponding vapor values. As seen in the data set presented in this study, only a small amount of seawater in the measured regions falls near the $\delta^{18}O = \delta^{2}H = 0‰$ isotopic composition (the Subpolar Gyre waters), and there are large areas where heightened freshwater content causes isotopic excursions beyond the range in these gridded data sets. Depending on the scientific question and the spatial and/or temporal scale of the research topic, there will be cases where it is important to consider a wider range of seawater isotopic values than is typically used.

Conflict of Interest

The authors declare no conflicts of interest relevant to this study.

Data Availability Statement

Seawater isotopic data is available at the NSF Arctic Data Center by Kopec et al. (2022). Data for the cruise seawater composition is available at the Rolling Deck to Repository for USCGC Healy segments HLY21TD and HLY2101 (Rolling Deck to Repository, 2021a, 2021b). Precipitation data from the Greenland Ecosystem Monitoring Programme were provided by Asiaq—Greenland Survey, Nuuk (Greenland Ecosystem Monitoring, 2022).

Acknowledgments
This work was supported by the US National Science Foundation (NSF) under award 2133156 to Jeffrey Welker, Douglas Causey, Eric Klein, and Ben Kopec. This work was also supported by the University of Oulu, Arctic Interaction, High Risk-High Reward award to Jeffrey Welker, Hannah Bailey, Alun Hubbard, and Hannu Marttila. In addition, support by Jeffrey Welker's UArctic Research Chairship was instrumental in the success of this research. Hannah Bailey was supported by the Research Council of Finland (Grant 348536). Alun Hubbard gratefully acknowledges an Arctic Five Chair (UiT), funding from the Research Council of Norway through its Centers of Excellence scheme (projects 223259 & 332635), and an ArcI research fellowship from the University of Oulu funded by the Academy of Finland PROFI4 (Grant 318930) and the FARIA network. The authors thank the US Coast Guard crew for their dedicated support of the research work throughout the cruise. The authors thank the Ship-based Science Technical Support in the Arctic (STARC) for maintaining and operating instrumentation throughout the cruise. In particular, the authors are grateful for the support of Brendon Mendenhall of STARC who helped coordinate the logistics of setting up the Picarro analyzers on the USCGC Healy and building the apparatus used to house these instruments during the cruise. We thank Xiahong Feng for providing isotopic data of daily precipitation from Ikerasaarsuk, Greenland, and Stephen Paulli Andersen and the students at the school in Ikerassarsuk for collecting these precipitation samples. We thank Robert Pickart for insightful discussions and support on the Healy. The authors thank the anonymous reviewers whose constructive comments resulted in the improvement of this manuscript.

References

Alkire, M. B., Morison, J., Schweiger, A., Zhang, J., Steele, M., Peralta-Ferriz, C., & Dickinson, S. (2017). A meteoric water budget for the Arctic Ocean. *Journal of Geophysical Research: Oceans*, *122*(12), 10020–10041. https://doi.org/10.1002/2017JC012807

Arrigo, K. R., & van Dijken, G. L. (2015). Continued increases in Arctic Ocean primary production. *Progress in Oceanography*, *136*, 60–70. https://doi.org/10.1016/j.pocean.2015.05.002

Bailey, H., Hubbard, A., Klein, E. S., Mustonen, K. R., Akers, P. D., Marttila, H., & Welker, J. M. (2021). Arctic sea-ice loss fuels extreme European snowfall. *Nature Geoscience*, *14*(5), 283–288. https://doi.org/10.1038/s41561-021-00719-y

Bamber, J., Van Den Broeke, M., Ettema, J., Lenaerts, J., & Rignot, E. (2012). Recent large increases in freshwater fluxes from Greenland into the North Atlantic. *Geophysical Research Letters*, *39*(19), L19501. https://doi.org/10.1029/2012GL052552

Bauch, D., Erlenkeuser, H., & Andersen, N. (2005). Water mass processes on Arctic shelves as revealed from $\delta^{18}O$ of H_2O. *Global and Planetary Change*, *48*(1–3), 165–174. https://doi.org/10.1016/j.gloplacha.2004.12.011

Bauch, D., Schlosser, P., & Fairbanks, R. G. (1995). Freshwater balance and the sources of deep and bottom waters in the Arctic Ocean inferred from the distribution of $H_2{}^{18}O$. *Progress in Oceanography*, *35*(1), 53–80. https://doi.org/10.1016/0079-6611(95)00005-2

Bendtsen, J., Mortensen, J., Lennert, K., & Rysgaard, S. (2015). Heat sources for glacial ice melt in a west Greenland tidewater outlet glacier fjord: The role of subglacial freshwater discharge. *Geophysical Research Letters*, *42*(10), 4089–4095. https://doi.org/10.1002/2015GL063846

Bonne, J. L., Behrens, M., Meyer, H., Kipfstuhl, S., Rabe, B., Schönicke, L., et al. (2019). Resolving the controls of water vapour isotopes in the Atlantic sector. *Nature Communications*, *10*(1), 1–10. https://doi.org/10.1038/s41467-019-09242-6

Box, J. E., Hubbard, A., Bahr, D. B., Colgan, W. T., Fettweis, X., Mankoff, K. D., et al. (2022). Greenland ice sheet climate disequilibrium and committed sea-level rise. *Nature Climate Change*, *12*(9), 808–813. https://doi.org/10.1038/s41558-022-01441-2

Brady, E., Stevenson, S., Bailey, D., Liu, Z., Noone, D., Nusbaumer, J., et al. (2019). The connected isotopic water cycle in the Community Earth System Model version 1. *Journal of Advances in Modeling Earth Systems*, *11*(8), 2547–2566. https://doi.org/10.1029/2019MS001663

Carmack, E. C., Yamamoto-Kawai, M., Haine, T. W., Bacon, S., Bluhm, B. A., Lique, C., et al. (2016). Freshwater and its role in the Arctic Marine System: Sources, disposition, storage, export, and physical and biogeochemical consequences in the Arctic and global oceans. *Journal of Geophysical Research: Biogeosciences*, *121*(3), 675–717. https://doi.org/10.1002/2015JG003140

Carroll, D., Sutherland, D. A., Curry, B., Nash, J. D., Shroyer, E. L., Catania, G. A., et al. (2018). Subannual and seasonal variability of Atlantic-origin waters in two adjacent west Greenland fjords. *Journal of Geophysical Research: Oceans*, *123*(9), 6670–6687. https://doi.org/10.1029/2018JC014278

Casado, M., Landais, A., Masson-Delmotte, V., Genthon, C., Kerstel, E., Kassi, S., et al. (2016). Continuous measurements of isotopic composition of water vapour on the East Antarctic Plateau. *Atmospheric Chemistry and Physics*, *16*(13), 8521–8538. https://doi.org/10.5194/acp-16-8521-2016

Charette, M. A., Kipp, L. E., Jensen, L. T., Dabrowski, J. S., Whitmore, L. M., Fitzsimmons, J. N., et al. (2020). The Transpolar Drift as a source of riverine and shelf-derived trace elements to the central Arctic Ocean. *Journal of Geophysical Research: Oceans*, *125*(5), e2019JC015920. https://doi.org/10.1029/2019JC015920

Chauché, N., Hubbard, A., Gascard, J. C., Box, J. E., Bates, R., Koppes, M., et al. (2014). Ice–ocean interaction and calving front morphology at two west Greenland tidewater outlet glaciers. *The Cryosphere*, *8*(4), 1457–1468. https://doi.org/10.5194/tc-8-1457-2014

Codispoti, L. A., Kelly, V., Thessen, A., Matrai, P., Suttles, S., Hill, V., et al. (2013). Synthesis of primary production in the Arctic Ocean: III. Nitrate and phosphate based estimates of net community production. *Progress in Oceanography*, *110*, 126–150. https://doi.org/10.1016/j.pocean.2012.11.006

Cooper, L. W., Magen, C., & Grebmeier, J. M. (2022). Changes in the oxygen isotope composition of the Bering Sea contribution to the Arctic Ocean are an independent measure of increasing freshwater fluxes through the Bering Strait. *PLoS One*, *17*(8), e0273065. https://doi.org/10.1371/journal.pone.0273065

Csank, A. Z., Czimczik, C. I., Xu, X., & Welker, J. M. (2019). Seasonal patterns of riverine carbon sources and export in NW Greenland. *Journal of Geophysical Research: Biogeosciences*, *124*(4), 840–856. https://doi.org/10.1029/2018JG004895

Curry, B., Lee, C. M., Petrie, B., Moritz, R. E., & Kwok, R. (2014). Multiyear volume, liquid freshwater, and sea ice transports through Davis Strait, 2004–10. *Journal of Physical Oceanography*, *44*(4), 1244–1266. https://doi.org/10.1175/JPO-D-13-0177.1

Dansgaard, W. (1964). Stable isotopes in precipitation. *Tellus*, *16*(4), 436–468. https://doi.org/10.1111/j.2153-3490.1964.tb00181.x

Dubinina, E. O., Kossova, S. A., & Miroshnikov, A. Y. (2019). Sources and mechanisms of seawater freshening in Tsivolky and Sedov bays (Novaya Zemlya Archipelago) based on isotope data (δD and $\delta^{18}O$). *Oceanology*, *59*(6), 836–847. https://doi.org/10.1134/S0001437019060043

Eicken, H., Krouse, H. R., Kadko, D., & Perovich, D. K. (2002). Tracer studies of pathways and rates of meltwater transport through Arctic summer sea ice. *Journal of Geophysical Research*, *107*(C10), SHE-22. https://doi.org/10.1029/2000JC000583

Farmer, J. R., Sigman, D. M., Granger, J., Underwood, O. M., Fripiat, F., Cronin, T. M., et al. (2021). Arctic Ocean stratification set by sea level and freshwater inputs since the last ice age. *Nature Geoscience*, *14*(9), 684–689. https://doi.org/10.1038/s41561-021-00789-y

Feng, D., Gleason, C. J., Lin, P., Yang, X., Pan, M., & Ishitsuka, Y. (2021). Recent changes to Arctic river discharge. *Nature Communications*, *12*(1), 1–9. https://doi.org/10.1038/s41467-021-27228-1

Forryan, A., Bacon, S., Tsubouchi, T., Torres-Valdés, S., & Naveira Garabato, A. C. (2019). Arctic freshwater fluxes: Sources, tracer budgets and inconsistencies. *The Cryosphere*, *13*(8), 2111–2131. https://doi.org/10.5194/tc-13-2111-2019

Fu, W., Moore, J. K., Primeau, F. W., Lindsay, K., & Randerson, J. T. (2020). A growing freshwater lens in the Arctic Ocean with sustained climate warming disrupts marine ecosystem function. *Journal of Geophysical Research: Biogeosciences*, *125*(12), e2020JG005693. https://doi.org/10.1029/2020JG005693

Gibson, J. J., Holmes, T., Stadnyk, T. A., Birks, S. J., Eby, P., & Pietroniro, A. (2020). ^{18}O and ^{2}H in streamflow across Canada. *Journal of Hydrology: Regional Studies*, *32*, 100754. https://doi.org/10.1016/j.ejrh.2020.100754

Greenland Ecosystem Monitoring. (2022). ClimateBasis Disko - Precipitation - Precipitation - 60min sample (mm) [Dataset]. *Greenland Ecosystem Monitoring Database*. https://doi.org/10.17897/638X-3Z89

Henson, H., Holding, J., Meire, L., Rysgaard, S., Stedmon, C., Stuart-Lee, A., et al. (2022). Carbonate chemistry and $\delta^{18}O$-H_2O from East and West Greenland fjords, August 2018 and 2016 [Dataset]. *Zenodo*. https://doi.org/10.5281/zenodo.6759882

Henson, H., Holding, J. M., Meire, L., Rysgaard, S., Stedmon, C., Stuart-Lee, A., et al. (2023). Coastal freshening drives acidification state in Greenland fjords. *Science of the Total Environment*, *855*, 158962. https://doi.org/10.1016/j.scitotenv.2022.158962

Hersbach, H., Bell, B., Berrisford, P., Biavati, G., Horányi, A., Muñoz Sabater, J., et al. (2023). *ERA5 monthly averaged data on single levels from 1940 to present*. Copernicus Climate Change Service (C3S) Climate Data Store (CDS). https://doi.org/10.24381/cds.f17050d7

Holding, J. M., Duarte, C. M., Sanz-Martín, M., Mesa, E., Arrieta, J. M., Chierici, M., et al. (2015). Temperature dependence of CO_2-enhanced primary production in the European Arctic Ocean. *Nature Climate Change*, *5*(12), 1079–1082. https://doi.org/10.1038/nclimate2768

Hopwood, M. J., Carroll, D., Browning, T. J., Meire, L., Mortensen, J., Krisch, S., & Achterberg, E. P. (2018). Non-linear response of summertime marine productivity to increased meltwater discharge around Greenland. *Nature Communications*, *9*(1), 1–9. https://doi.org/10.1038/s41467-018-05488-8

Huhn, O., Rhein, M., Kanzow, T., Schaffer, J., & Sültenfuß, J. (2021). Submarine meltwater from Nioghalvfjerdsbræ (79 North Glacier), Northeast Greenland. *Journal of Geophysical Research: Oceans*, *126*(7), e2021JC017224. https://doi.org/10.1029/2021JC017224

Kanna, N., Sugiyama, S., Ohashi, Y., Sakakibara, D., Fukamachi, Y., & Nomura, D. (2018). Upwelling of macronutrients and dissolved inorganic carbon by a subglacial freshwater driven plume in Bowdoin Fjord, northwestern Greenland. *Journal of Geophysical Research: Biogeosciences*, *123*(5), 1666–1682. https://doi.org/10.1029/2017JG004248

Karlsson, N. B., Solgaard, A. M., Mankoff, K. D., Gillet-Chaulet, F., MacGregor, J. A., Box, J. E., et al. (2021). A first constraint on basal melt-water production of the Greenland ice sheet. *Nature Communications*, *12*(1), 1–10. https://doi.org/10.1038/s41467-021-23739-z

Klein, E. S., Baltensperger, A. P., & Welker, J. M. (2024). Complexity of Arctic Ocean water isotope ($\delta^{18}O$, $\delta^{2}H$) spatial and temporal patterns revealed with machine learning. *Elementa: Science of the Anthropocene*, *12*(1), 00127. https://doi.org/10.1525/elementa.2022.00127

Kopec, B. G., Feng, X., Michel, F. A., & Posmentier, E. S. (2016). Influence of sea ice on Arctic precipitation. *Proceedings of the National Academy of Sciences*, *113*(1), 46–51. https://doi.org/10.1073/pnas.1504633113

Kopec, B. G., Feng, X., Posmentier, E. S., Chipman, J. W., & Virginia, R. A. (2018). Use of principal component analysis to extract environmental information from lake water isotopic compositions. *Limnology & Oceanography*, *63*(3), 1340–1354. https://doi.org/10.1002/lno.10776

Kopec, B. G., Klein, E. S., & Welker, J. M. (2022). Continuous seawater isotopic ($\delta^{18}O$, δD, and d-excess) observations from 2021 Arctic cruise on United States Coast Guard Cutter Healy [Dataset]. *Arctic Data Center*. https://doi.org/10.18739/A24J09Z7K

Lee, J. E., Fung, I., DePaolo, D. J., & Henning, C. C. (2007). Analysis of the global distribution of water isotopes using the NCAR atmospheric general circulation model. *Journal of Geophysical Research*, *112*(D16), D16306. https://doi.org/10.1029/2006JD007657

LeGrande, A. N., & Schmidt, G. A. (2006). Global gridded data set of the oxygen isotopic composition in seawater. *Geophysical Research Letters*, *33*(12), L12604. https://doi.org/10.1029/2006GL026011

Lesack, L. F., & Marsh, P. (2010). River-to-lake connectivities, water renewal, and aquatic habitat diversity in the Mackenzie River Delta. *Water Resources Research*, *46*(12), W12504. https://doi.org/10.1029/2010WR009607

Lewis, K. M., Van Dijken, G. L., & Arrigo, K. R. (2020). Changes in phytoplankton concentration now drive increased Arctic Ocean primary production. *Science*, *369*(6500), 198–202. https://doi.org/10.1126/science.aay8380

Lin, P., Pickart, R. S., McRaven, L. T., Arrigo, K. R., Bahr, F., Lowry, K. E., et al. (2019). Water mass evolution and circulation of the northeastern Chukchi Sea in summer: Implications for nutrient distributions. *Journal of Geophysical Research: Oceans*, *124*(7), 4416–4432. https://doi.org/10.1029/2019JC015185

Macdonald, R. W., Paton, D. W., Carmack, E. C., & Omstedt, A. (1995). The freshwater budget and under-ice spreading of Mackenzie River water in the Canadian Beaufort Sea based on salinity and $^{18}O/^{16}O$ measurements in water and ice. *Journal of Geophysical Research*, *100*(C1), 895–919. https://doi.org/10.1029/94JC02700

MacLachlan, S. E., Cottier, F. R., Austin, W. E., & Howe, J. A. (2007). The salinity: $\delta^{18}O$ water relationship in Kongsfjorden, western Spitsbergen. *Polar Research*, *26*(2), 160–167. https://doi.org/10.1111/j.1751-8369.2007.00016.x

Mathieu, R., Pollard, D., Cole, J. E., White, J. W., Webb, R. S., & Thompson, S. L. (2002). Simulation of stable water isotope variations by the GENESIS GCM for modern conditions. *Journal of Geophysical Research*, *107*(D4), ACL-2. https://doi.org/10.1029/2001JD900255

Meire, L., Mortensen, J., Meire, P., Juul-Pedersen, T., Sejr, M. K., Rysgaard, S., et al. (2017). Marine-terminating glaciers sustain high productivity in Greenland fjords. *Global Change Biology*, *23*(12), 5344–5357. https://doi.org/10.1111/gcb.13801

Mellat, M., Bailey, H., Mustonen, K. R., Marttila, H., Klein, E. S., Gribanov, K., et al. (2021). Hydroclimatic controls on the isotopic ($\delta^{18}O$, $\delta^{2}H$, *d-excess*) traits of Pan-Arctic summer rainfall events. *Frontiers in Earth Science*, *9*, 651731. https://doi.org/10.3389/feart.2021.651731

Mellat, M., Brunello, C. F., Werner, M., Bauch, D., Damm, E., Angelopoulos, M., et al. (2024). Isotopic signatures of snow, sea ice, and surface seawater in the central Arctic Ocean during the MOSAiC expedition. *Elementa: Science of the Anthropocene*, *12*(1), 00078. https://doi.org/10.1525/elementa.2023.00078

Meneghello, G., Marshall, J., Timmermans, M. L., & Scott, J. (2018). Observations of seasonal upwelling and downwelling in the Beaufort Sea mediated by sea ice. *Journal of Physical Oceanography*, *48*(4), 795–805. https://doi.org/10.1175/JPO-D-17-0188.1

Morison, J., Kwok, R., Dickinson, S., Andersen, R., Peralta-Ferriz, C., Morison, D., et al. (2021). The cyclonic mode of Arctic Ocean circulation. *Journal of Physical Oceanography*, *51*(4), 1053–1075. https://doi.org/10.1175/JPO-D-20-0190.1

Mortensen, J., Bendtsen, J., Motyka, R. J., Lennert, K., Truffer, M., Fahnestock, M., & Rysgaard, S. (2013). On the seasonal freshwater stratification in the proximity of fast-flowing tidewater outlet glaciers in a sub-Arctic sill fjord. *Journal of Geophysical Research: Oceans*, *118*(3), 1382–1395. https://doi.org/10.1002/jgrc.20134

Mote, T. L. (2014). MEaSUREs Greenland surface melt daily 25km EASE-grid 2.0, Version 1 [Dataset]. *National Snow and Ice Data Center Distributed Active Archive Center*. https://doi.org/10.5067/MEASURES/CRYOSPHERE/nsidc-0533.001

Mote, T. L., & Anderson, M. R. (1995). Variations in snowpack melt on the Greenland ice sheet based on passive-microwave measurements. *Journal of Glaciology*, *41*(137), 51–60. https://doi.org/10.3189/S0022143000017755

Nusbaumer, J., Wong, T. E., Bardeen, C., & Noone, D. (2017). Evaluating hydrological processes in the Community Atmosphere Model Version 5 (CAM5) using stable isotope ratios of water. *Journal of Advances in Modeling Earth Systems*, *9*(2), 949–977. https://doi.org/10.1002/2016MS000839

Paquette, R. A., & Bourke, R. H. (1974). Observations on the coastal current of Arctic Alaska. *Journal of Marine Research*, *32*, 195–207.

Pasqualini, A., Schlosser, P., Newton, R., & Koffman (2017). T. N. U.S. GEOTRACES Arctic section ocean water hydrogen and oxygen stable isotope analyses, Version 1.0. *Interdisciplinary Earth Data Alliance*. https://doi.org/10.1594/IEDA/100633

Polyakov, I. V., Pnyushkov, A. V., Alkire, M. B., Ashik, I. M., Baumann, T. M., Carmack, E. C., et al. (2017). Greater role for Atlantic inflows on sea-ice loss in the Eurasian Basin of the Arctic Ocean. *Science*, *356*(6335), 285–291. https://doi.org/10.1126/science.aai8204

Polyakov, I. V., Pnyushkov, A. V., & Carmack, E. C. (2018). Stability of the Arctic halocline: A new indicator of Arctic climate change. *Environmental Research Letters*, *13*(12), 125008. https://doi.org/10.1088/1748-9326/aaec1e

Putman, A. L., Feng, X., Sonder, L. J., & Posmentier, E. S. (2017). Annual variation in event-scale precipitation δ^2H at Barrow, AK, reflects vapor source region. *Atmospheric Chemistry and Physics*, *17*(7), 4627–4639. https://doi.org/10.5194/acp-17-4627-2017

Rantanen, M., Karpechko, A. Y., Lipponen, A., Nordling, K., Hyvärinen, O., Ruosteenoja, K., et al. (2022). The Arctic has warmed nearly four times faster than the globe since 1979. *Communications Earth & Environment*, *3*(1), 168. https://doi.org/10.1038/s43247-022-00498-3

Reverdin, G., Niiler, P. P., & Valdimarsson, H. (2003). North Atlantic Ocean surface currents. *Journal of Geophysical Research*, *108*(C1), 2-1. https://doi.org/10.1029/2001JC001020

Rolling Deck to Repository. (2021a). HLY2101 [Dataset]. *Rolling Deck to Repository*. https://doi.org/10.7284/909350

Rolling Deck to Repository. (2021b). HLY21TD [Dataset]. *Rolling Deck to Repository*. https://doi.org/10.7284/909349

Rudels, B., Anderson, L. G., & Jones, E. P. (1996). Formation and evolution of the surface mixed layer and halocline of the Arctic Ocean. *Journal of Geophysical Research*, *101*(C4), 8807–8821. https://doi.org/10.1029/96JC00143

Rysgaard, S., Boone, W., Carlson, D., Sejr, M. K., Bendtsen, J., Juul-Pedersen, T., et al. (2020). An updated view on water masses on the pan-west Greenland continental shelf and their link to proglacial fjords. *Journal of Geophysical Research: Oceans*, *125*(2), e2019JC015564. https://doi.org/10.1029/2019JC015564

Schmidt, G. A., LeGrande, A. N., & Hoffmann, G. (2007). Water isotope expressions of intrinsic and forced variability in a coupled ocean-atmosphere model. *Journal of Geophysical Research*, *112*(D10), D10103. https://doi.org/10.1029/2006JD007781

Steen-Larsen, H. C., Johnsen, S. J., Masson-Delmotte, V., Stenni, B., Risi, C., Sodemann, H., et al. (2013). Continuous monitoring of summer surface water vapor isotopic composition above the Greenland Ice Sheet. *Atmospheric Chemistry and Physics*, *13*(9), 4815–4828. https://doi.org/10.5194/acpd-13-1399-2013

Strauss, J., Biasi, C., Sanders, T., Abbott, B. W., von Deimling, T. S., Voigt, C., et al. (2022). A globally relevant stock of soil nitrogen in the Yedoma permafrost domain. *Nature Communications*, *13*(1), 1–9. https://doi.org/10.1038/s41467-022-33794-9

Sutherland, D. A., Pickart, R. S., Peter Jones, E., Azetsu-Scott, K., Jane Eert, A., & Ólafsson, J. (2009). Freshwater composition of the waters off southeast Greenland and their link to the Arctic Ocean. *Journal of Geophysical Research*, *114*(C5), C05020. https://doi.org/10.1029/2008JC004808

Terhaar, J., Lauerwald, R., Regnier, P., Gruber, N., & Bopp, L. (2021). Around one third of current Arctic Ocean primary production sustained by rivers and coastal erosion. *Nature Communications*, *12*(1), 1–10. https://doi.org/10.1038/s41467-020-20470-z

The Arctic Great Rivers Observatory. (2024). Arctic Great Rivers Observatory biogeochemistry and discharge data, North America and Siberia, 2003 – 2024 [Dataset]. *Arctic Data Center*. https://doi.org/10.18739/A2BC3SZ84

Tian, L., Gao, Y., Ackley, S. F., Stammerjohn, S., Maksym, T., & Weissling, B. (2018). Stable isotope clues to the formation and evolution of refrozen melt ponds on Arctic sea ice. *Journal of Geophysical Research: Oceans*, *123*(12), 8887–8901. https://doi.org/10.1029/2018JC013797

Timmermans, M. L., & Marshall, J. (2020). Understanding Arctic Ocean circulation: A review of ocean dynamics in a changing climate. *Journal of Geophysical Research: Oceans*, *125*(4), e2018JC014378. https://doi.org/10.1029/2018JC014378

U.S. National Ice Center and National Snow and Ice Data Center. (2010). *Multisensor analyzed Sea Ice Extent - Northern Hemisphere (MASIE-NH), Version 1*. [Indicate subset used]. Compiled by F. Fetterer, M. Savoie, S. Helfrich, and P. Clemente-Colón. National Snow and Ice Data Center. Updated daily. https://doi.org/10.7265/N5GT5K3K

Weingartner, T. J., Danielson, S. L., & Royer, T. C. (2005). Freshwater variability and predictability in the Alaska Coastal Current. *Deep Sea Research Part II: Topical Studies in Oceanography*, *52*(1–2), 169–191. https://doi.org/10.1016/j.dsr2.2004.09.030

Woodgate, R. A. (2018). Increases in the Pacific inflow to the Arctic from 1990 to 2015, and insights into seasonal trends and driving mechanisms from year-round Bering Strait mooring data. *Progress in Oceanography*, *160*, 124–154. https://doi.org/10.1016/j.pocean.2017.12.007

Yamamoto-Kawai, M., McLaughlin, F. A., Carmack, E. C., Nishino, S., & Shimada, K. (2008). Freshwater budget of the Canada Basin, Arctic Ocean, from salinity, δ^{18}O, and nutrients. *Journal of Geophysical Research*, *113*(C1), C01007. https://doi.org/10.1029/2006JC003858

Yamamoto-Kawai, M., McLaughlin, F. A., Carmack, E. C., Nishino, S., Shimada, K., & Kurita, N. (2009). Surface freshening of the Canada Basin, 2003–2007: River runoff versus sea ice meltwater. *Journal of Geophysical Research*, *114*(C1), C00A05. https://doi.org/10.1029/2008JC005000

Yi, Y., Gibson, J. J., Cooper, L. W., Hélie, J. F., Birks, S. J., McClelland, J. W., et al. (2012). Isotopic signals (^{18}O, ^{2}H, ^{3}H) of six major rivers draining the pan-Arctic watershed. *Global Biogeochemical Cycles*, *26*(1), GB1027. https://doi.org/10.1029/2011GB004159

Yi, Y., Gibson, J. J., Hélie, J. F., & Dick, T. A. (2010). Synoptic and time-series stable isotope surveys of the Mackenzie River from Great Slave Lake to the Arctic Ocean, 2003 to 2006. *Journal of Hydrology*, *383*(3–4), 223–232. https://doi.org/10.1016/j.jhydrol.2009.12.038

Zhang, J., Weijer, W., Steele, M., Cheng, W., Verma, T., & Veneziani, M. (2021). Labrador Sea freshening linked to Beaufort Gyre freshwater release. *Nature Communications*, *12*(1), 1229. https://doi.org/10.1038/s41467-021-21470-3

References From the Supporting Information

Climate Reanalyzer. (n.d.). *[Monthly reanalysis maps]*. Climate Change Institute, University of Maine. Retrieved from https://climtereanalyzer.org/